Synthesis and Characterization of Fe_2O_3/NiO/C Nanocomposite for Photocatalytic Degradation of Methylene Blue

Abinet Mekonnen Haile

A Thesis Submitted to the Department of Applied Chemistry
College of Applied Natural Science

Presented in Partial Fulfillment of the Requirement for the Degree of
Master of Science in Applied Chemistry (Industrial Chemistry)

Office of Graduate Studies
Adama Science and Technology University

June, 2025
Adama, Ethiopia

Synthesis and Characterization of Fe_2O_3/NiO/C Nanocomposite for Photocatalytic Degradation of Methylene Blue

Abinet Mekonnen Haile

Major Advisor: Nejat Redwan (PhD)

Co-advisor: Hizkeal Tsade (PhD)

A Thesis Submitted to the Department of Applied Chemistry
College of Applied Natural Science

Presented in Partial Fulfillment of the Requirement for the Degree of Master of Science in Applied Chemistry (Industrial Chemistry)

Office of Graduate Studies
Adama Science and Technology University

June, 2025
Adama, Ethiopia

DECLARATION

I declare that this Master's thesis entitled “**Synthesis and Characterization of Fe_2O_3/NiO/C Nanocomposite for Photocatalytic Degradation of Methylene Blue**” is my original work. This work is my own and has not been submitted for any academic degree, diploma, or certificate in any other university. All sources of materials that are used for this thesis have been duly acknowledged through proper citations.

Abinet Mekonnen Haile 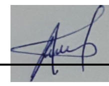 12/06/2025

Name of Student Signature Date

RECOMMENDATION

We, the advisors of this thesis, hereby certify that we have read the revised version of the thesis entitled "**Synthesis and Characterization of Fe_2O_3/NiO/C Nanocomposite for Photocatalytic Degradation of Methylene Blue**" prepared under our guidance by Abinet Mekonnen Haile submitted in partial fulfillment of the requirements for the degree of Master's of Science in Applied Chemistry (Industrial Chemistry). Therefore, we recommend the submission of the revised version of the thesis to the department following the applicable procedures.

Nejat Redwan (PhD)		12/06/2025
Major Advisor	Signature	Date
Hizkeal Tsade		12/6/2025
Co-Advisor	Signature	Date

APPROVAL PAGE

We, the advisors of the thesis entitled "**Synthesis and Characterization of Fe_2O_3/NiO/C Nanocomposite for Photocatalytic Degradation of Methylene Blue**" and developed by Abinet Mekonnen Haile, hereby certify that the recommendations and suggestions made by the board of examiners are appropriately incorporated into the final version of the thesis.

Nejat Redwan (PhD)	______________	12/06/2025
Major Advisor	Signature	Date
Hizkeal Tsade (PhD)	______________	12/06/2025
Co-advisor	Signature	Date

We, the undersigned, members of the Board of Examiners of the thesis by Abinet Mekonnen Haile have read and evaluated the thesis entitled "**Synthesis and Characterization of Fe_2O_3/NiO/C Nanocomposite for Photocatalytic Degradation of Methylene Blue**" and examined the candidate during open defense. This is, therefore, to certify that the thesis is accepted for partial fulfillment of the requirement of the degree of Master of Science in Applied Chemistry (Industrial Chemistry).

Gemechu Deressa (PhD)	______________	12/06/2025
Chairperson	Signature	Date
Aschalew Tadesse (PhD)	______________	12/06/2025
Internal Examiner	Signature	Date
Dejene Disasa (PhD)	______________	12/06/2025
External Examiner	Signature	Date

Final approval and acceptance of the thesis is contingent upon submission of its final copy to the Office of Postgraduate Studies (OPGS) through the Department Graduate Council (DGC) and College Graduate Committee (CGC).

______________	______________	______________
Department Head	Signature	Date
______________	______________	______________
College Dean	Signature	Date
______________	______________	______________
Office of Postgraduate Studies, Dean	Signature	Date

ACKNOWLEDGMENT

First, I would like to express my thanks to the Department of Applied Chemistry, College of Applied Natural Science, Adama Science and Technology University, for hosting and providing facilities. I would like to extend my heartfelt gratitude to my advisor, Nejat Redwan (PhD), for her unwavering support and invaluable direction throughout my thesis research. My thanks go for my co-advisor Hitskeal Tsade (PhD) for his comments and suggestions. I am deeply thankful to Bzuayehu Abebe (PhD), Getye Behailu (PhD) and Mr. Yenebeb Haftu for their comments in data interpretations. My sincere thanks also go to the head of the Department of Applied chemistry, Gemechu Deressa (PhD) for his administrative support and for fostering a conducive atmosphere for graduate research. I am profoundly thankful to God for granting me the time, health, strength,and patience to complete my M.Sc. study successfully. Special thanks go for academic technical, Mr. Demeke Tessfaye, Mr. Guta Amanu and Mr. Girma Hailu for their support in my thesis work. I would like to acknowledge my friend Rahel Abera for her ideas support as well in materials. Lastly, I would like to express my heartfelt gratitude to all my family members and close friends for their encouragement and support throughout this research.

TABLE OF CONTENTS

LIST OF TABLES

LIST OF FIGURES

LIST OF ABBREVIATIONS

AC	Activated carbon
CV	Conduction band
CFs	Carbon fibers
CNTs	Carbon nanotubes
CSs	Carbon sphere
FESEM	Field emission scanning electron microscopy
FTIR	Fourier transform infrared
MB	Methylene blue
MO	Methylene orange
PL	Photoluminescence
SC	Semiconductor
SCGs	Spent coffee grounds
VB	Valence band
XRD	X-ray diffraction

ABSTRACT

Wastewater generated from textile industries mostly consists of the persistent synthetic organic dye, particularly methylene blue (MB), released to the environment before treatment has a significant trouble because of its adverse effects on human life and aquatic ecosystems. A variety of treatment techniques have been broadly employed to remove pollutants from the environment. Photocatalysis is one of the methods that possesses several advantages. In this study, the co-precipitation method was used to synthesize Fe_2O_3*/NiO/C nanocomposites, with spent coffee grounds (SCGs) as the carbon source. Different molar ratio of precursor salts* $Fe(NO_3)_3.9H_2O$ *(0.2M, 0.1M, and 0.2 M) and* $Ni(NO_3)_2.6H_2O$ *(0.2M, 0.2M, 0.1M) were used, combined with 0.2 g carbon, corresponding to (1:1)C, (1:2)C and (2:1)C ratio, respectively. Then, the synthesized nanocomposites were characterized using XRD, FESEM-EDX, FTIR, UV-Vis DRS, and PL analytical techniques. From the XRD result, the average crystalline size was found to be 19.89, 13.22, and 15.86 nm for* Fe_2O_3*/NiO/C (1:1)C, (1:2)C, and (2:1)C composites. The elemental composition and morphology were analyzed by FESEM-EDX analysis. The energy band gap was approximated to be 2.44, 2.47, and 2.43 eV for (1:1)C, (1:2)C, and (2:1)C nanocomposites. FTIR results showed the stretching of Fe-O and Ni-O bonds in* α*-*Fe_2O_3 *and NiO in the synthesized (1:2)C nanocomposites. From the PL result, the (1:2)C composite showed the lowest PL intensity in comparison with (1:1)C, and (2:1)C indicated hindrance of electron-hole recombination (EHR). The degradation efficiency of synthesized nanocomposites was found to be 80.23%, 91.65%, and 87.22% for the (1:1)C, (1:2)C, and (2:1)C nanocomposites. Among these, (1:2)C sample showed the highest degradation efficiency due to lower electron-hole recombination and was selected for photodegradation of MB. The improved photodegradation of MB was estimated to be 93.35% using a 30 mg/L initial MB concentration, pH 9, 10 mg catalyst dosage, 30 min contact time, and a visible light source.*

Keywords: *Co-precipitation,* Fe_2O_3*/NiO/C, Methylene Blue, Nanocomposite, Photocatalysis*

CHAPTER ONE
INTRODUCTION

1.1. Background of the Study

The growing demand for synthetic dyes across many industries is among the most prominent drivers for increased production (Din, Khalid, Najeeb, & Hussain, 2021; Fobiri, 2022). Many synthetic dyes are applied in many areas, including paint, leather, food, paper, textiles, and pharmaceuticals as colorants (Din et al., 2021). The most significant application of synthetic dyes is in the textile industry (Alegbe & Uthman, 2024). However, many synthetic dyes resist biodegradation, which is an important environmental concern (Dehno Khalaji, 2022).

Methylene blue is a synthetic dye employed as a coloring material by various industries, including paper, wool, silk, cotton, food, textiles, cosmetics, and drugs, utilizing a lot of it in their products (I. Khan et al., 2022). However, the discharge of untreated (MB) containing wastewater from different industries is toxic to human and aquatic life health. MB causes many diseases like respiratory distress, gastrointestinal disorder, blindness, and mental instability (Hong, Bao, & Liu, 2025; Moorthy, Rathi, Shukla, Kumar, & Bharti, 2021). The negative effects related to wastewater with MB dyes then ensure the need for effective treatment before industrial disposal.

Researchers have reported numerous methods of eliminating MB dye from the environment because of the negative effects that it presents in the ecosystem, such as adsorption, biodegradation, chemical methods, coagulation, and ion-exchange methods (Bashir et al., 2019; Benalia et al., 2024). Even so, these procedures are usually linked to limitations like the requirement of expensive apparatus, lower efficiency, and producing secondary pollutants. In contrast, photocatalytic removal of toxic dye is advantageous with various aspects like the use of renewable sunlight, ease of operating techniques, efficient removal, and complete mineralization of the dye (D. Chen et al., 2020; Ebrahimzadeh, Mortazavi-Derazkola, & Zazouli, 2020).

Recently, researchers have been developing semiconductor photocatalysts using sustainable solar energy to satisfy both efficiency and economic needs (Alshehri, Al-Marzouki, Alshehrie, & Hafez, 2018; J. Chen et al., 2022). Semiconductors such as NiO, ZnO, CuO, TiO_2, and Fe_2O_3 can remove many organic pollutants with high photocatalytic performance (Sajid, Ishaq, Alomayri, Zhai, & Khan, 2025). Hematite (α-Fe_2O_3) has been regarded as the most favorable potential photocatalyst in recent years for the elimination of several hazardous organic pollutants (Keerthana et al., 2021), because of its availability, excellent stability, non-toxicity, and absorption of visible light, collecting up to 40 percent of the solar energy (C. Yao et al., 2023). However, the rapid charge carrier recombination of this α-Fe_2O_3 limits its use in photocatalysis.

The photocatalytic process typically begins when UV radiation strikes the oxide samples, causing electrons to be excited from the valence band (VB) to the conduction band (CB). This transition results in the formation of negative electrons and positive holes at the photocatalyst surface (Khalaf, Abu-Dalo, & AlShamaileh, 2024). These charge carriers are either combined or involved in the degradation of MB at the surface of the catalyst by a redox reaction (Nas-soko et al., 2012). The charge carriers recombination is considered the key electronic obstacles that limits the photocatalytic applications of single α-Fe_2O_3 (W. Huang, Zhang, & Wang, 2023). Researchers have made numerous efforts to address the limitations of α-Fe_2O_3 through various methods, including doping with different materials, modifying the surface, creating composites, and forming heterostructures (Sridharan et al., 2024).

Among these modification techniques, composites are a potent and effective way to create semiconductors that are photo-responsive in the visible spectrum (Khalaf et al., 2024). Nano-composite material is made up of many phases with at least one, two, or three dimensions that fall within the nanoscale range (Omanović-Mikličanin, Badnjević, Kazlagić, & Hajlovac, 2020). They can serve as a good photocatalyst due to their ability to separate charges, resistance to photo-corrosion, and propensity to capture visible light, producing synergistic effects and improved performance when compared to individual components (Suresh et al., 2023).

Semiconductors (α-Fe_2O_3) and (NiO) have a favorable energy band gap that enables them to capture visible light, ensuring them ideal options for photocatalytic uses (S. Khan, Ajmal, Mahmood, & ul Haq, 2023). NiO, a p-type semiconductor, has a wide band gap of 3.0- 4.0 eV, and it is used as an active catalytic material because of its good charge carrier mobility, thermodynamic stability, low recombination, remarkable photo sensitivity, and high optical properties (Mou et al., 2022). The composites of α-Fe_2O_3 and NiO are appropriate for photocatalytic applications due to their advantageous band gap energies, which enable them to absorb visible light (S. Khan et al., 2023). The photodegradation of Rose Bengal dye using α-Fe_2O_3/NiO (2:1) composite synthesized via the chemical co-precipitation method reported maximum degradation of 94% in 90 min (Devi et al., 2025). The reported high photocatalytic performance of α-Fe_2O_3/NiO (2:1) composite could be associated to synergistic effects between NiO and α-Fe_2O_3, which retards the photoexcited electron-holes recombination.

A nanocomposite might be synthesized using various methods. For instance, hydrothermal (Han et al., 2024), sol-gel (Ismail et al., 2019), and co-precipitation (Devi et al., 2025), among others. Co-precipitation is a favorable, straightforward, and common technique to achieve small particle size (Santoshi, Bharadwaj, Varma, Dhand, & Choudary, 2024). A study on the degradation of methylene blue and methylene orange dyes using γ-Fe_2O_3/AC (1:3) composite via co-precipitation method reported 94% in 180 min MO dye and 87% in 125 min MB dye (Faheem et al., 2024). The reported high photocatalytic activity of γ-Fe_2O_3/AC (1:3) composite could be related to synergistic effects between AC and α-Fe_2O_3, which retards the recombination of photogenerated charge carries.

Recently, a wide range of carbon-based material photocatalysts has been synthesized, such as carbon spheres (CSs) (A Boudjemaa et al., 2021), activated carbon (AC) (Bukhari et al., 2024), graphene (Lopes, Martins, Nogueira, Estrada, & Trindade, 2021), carbon nanotubes (CNTs) (Zhang et al., 2022), and carbon fibers (CFs) (M. Tahir, Alesayi, & Al Zahmi, 2023). They are well known to possess improved electron conductivity, chemical stability, excellent adsorption capacity, improved dispersion behavior, high surface area, and electrical conductivity (Baniamerian, Teimoori, & Saberi, 2021; Zou, Gao, Ok, & Dong, 2019). These advances increase their degradation of organic pollutants (Baniamerian et al., 2021; Han et al., 2024). Among these, activated carbon (AC), especially when derived from natural biopolymers or waste products, offers a workable and economical solution for synthetic dye degradation attributed its excellent porous structure, variable surface characteristic, high surface area, and low cost (Iwanow, Gärtner, Sieber, & König, 2020). Kadirova et al. synthesized Fe_2O_3 and

Fe_2O_3 /ACs by pore volume impregnation of AC in a solution of iron nitrate solution at 250 °C. The Fe_2O_3/ACs materials exhibited an enhanced photodegradation of MB dye (Kadirova et al., 2014). However, there are limited reports available on the carbonation of photocatalysts using Fe/Ni complexes. In this study, spent coffee grounds (SCGs) were chosen as the precursor for preparing carbon.

Therefore, this study aimed to synthesize Fe_2O_3/NiO/C nanocomposite using the co-precipitation method, to characterize the synthesized nanocomposite using XRD, UV-Vis DRS, PL, FESEM-EDX, and FTIR techniques, and investigate their application for photodegradation of MB dye.

1.2. Statement of the Problem

The chronic environmental pollution caused by synthetic dyes, particularly methylene blue (MB), has become a serious issue due to their adverse effects on living organisms (Cheng et al., 2020). Recent studies have reported that metal oxide catalysts, particularly hematite (α-Fe_2O_3), are promising materials for the elimination of organic dyes (Khalaf et al., 2024). However, the degradation performance of α-Fe_2O_3 is limited due to the fast charge carrier's recombination (Mishra & Chun, 2015). The inter-facial interaction between Fe_2O_3/NiO/C nanocomposite improves the electron-hole pairs separation, which improves the degradation of MB. However, the interaction between Fe_2O_3/NiO and carbon has not been widely applied, it likely enhances catalytic activity by improving the charge carrier's separation. Furthermore, the photocatalytic activity of such catalysts for MB dye degradation has yet to be explored. Therefore, the present study aimed to synthesize and characterize the Fe_2O_3/NiO/C nanocomposites using the co-precipitation method and evaluate their efficiency in MB dye degradation.

1.3. Objective of the Study

1.3.1. General objective

The general objective of this study was to synthesize and characterize Fe_2O_3/NiO/C nanocomposite for the photocatalytic degradation of methylene blue dye

1.3.2. Specific objectives

- To prepare carbon from spent coffee grounds
- To synthesize Fe_2O_3 /NiO nanocomposite using the co-precipitation method
- To synthesize Fe_2O_3/NiO/C nanocomposite using the co-precipitation methods
- To characterize the synthesized nanocomposite using FTIR, FESEM-EDX, UV-Vis DRS, PL, and XRD spectroscopies
- To investigate the photodegradation efficiency of the synthesized Fe_2O_3/NiO/C nano-composite for methylene blue dye

1.3.3. Significance of the study

This study showed a low-cost, environmentally sustainable solution for degrading methylene blue using Fe_2O_3/NiO/C composite. Furthermore, Fe_2O_3/NiO composite catalytic performance was enhanced by using carbon prepared from spent coffee grounds, providing efficient pollutant degradation and waste recycling. From the outcome of this study, all communities, the scientific community, industries, and future researchers will benefit. This research opens the door for further research on the carbonization of metal oxides with waste material-derived carbon.

1.4. Scope of the Study

The scope of this study was limited to the synthesized Fe_2O_3/NiO/C composite, and the synthesized composite was characterized by PL, FESEM-EDX, FTIR, UV-Vis DRS, and XRD techniques. Furthermore, the synthesized Fe_2O_3/NiO/C composite was examined for the efficiency of MB dye degradation.

CHAPTER TWO
2. LITERATURE REVIEW

2.1. Photocatalysis

The word photocatalysis combines the terms "phos," which means light, and "katatalyo, " which means to decompose (Rani, Nayak, & Sahu, 2022). Generally, photocatalysis describes alteration in the speed of a chemical process caused by visible light or ultraviolet light in the occurrence of a material that captures light and participates in chemical change of reactants. A material that captures visible or ultraviolet light and produces reactive species when excited is called a photocatalyst (Koe, Lee, Chong, Pang, & Sim, 2020).

The photocatalytic reactions can occur in either heterogeneous or homogeneous systems; however, heterogeneous photocatalysts have received a lot more interest. Because of its potential uses in numerous fields, including the cleanup of environments and the generation of energy. Furthermore, heterogeneous photocatalysts are easily separated from a reaction mixture, making them appropriate for application in additional reactions (Antonopoulou, 2022).

2.2. Principles of Heterogeneous Photocatalysis

Heterogeneous catalysts are defined as catalysts that exist in a different phase or state compared to the reactants involved in a chemical reaction. These catalysts typically consist of semiconductors that provide active sites for interaction with reactants within the reaction environment (Ruhul et al., 2015).

Heterogeneous photocatalysis refers to the improvement of photochemical reactions using a semiconductor catalyst. The process starts when an electron is excited from the valence band to the conduction band by a photon with energy that equals or greater than the semiconductor photocatalyst band gap. An electron - hole pair is created as the result of this excitation, with the electron migrating to the CB and the hole remaining in the VB (X. Yang & Wang, 2018). Superoxide radicals (O_2•) are created when the electron interacts with molecular oxygen on the catalyst surface. Meanwhile, the hole creates hydroxyl radicals (HO•) by oxidizing water and hydroxyl ions or organic molecules. These produced radicals are strong oxidants that react with organic contaminants, turning many of them into mineral acids, carbon dioxide, and water (H. Yang, 2021). The following steps can be used to summarize the photocatalysis mechanism: as illustrated in Fig. 1, the semiconductor undergoes the following process. i) The semiconductor absorbs light, ii) this absorption leads to the creation of charge carriers, iii) these photogenerated electron-hole pairs migrate and may recombine, iv) reactants get adsorbed onto the surface while products are desorbed, and v) the surface of the semiconductor is where redox reaction occur.

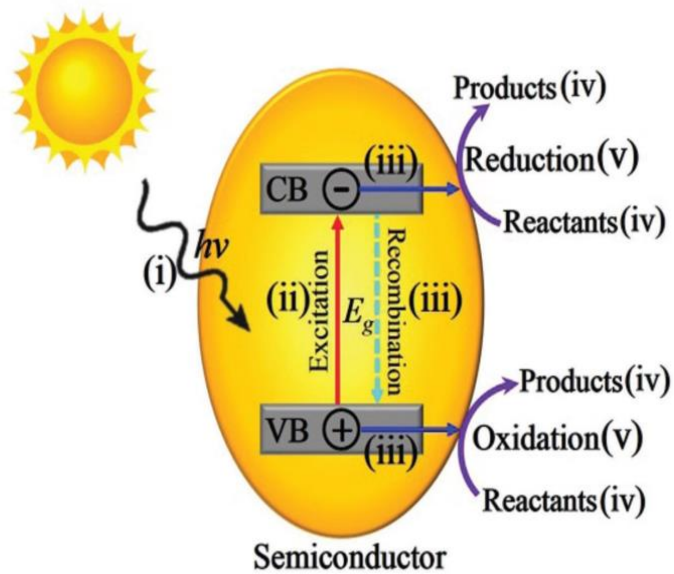

Figure 1: Photocatalysis (Low, Yu, Jaroniec, Wageh, & Al-Ghamdi, 2017)

2.2.1. Applications of heterogeneous photocatalysis

Heterogeneous photocatalysis is an inexpensive and environmentally sustainable method for producing hydrogen disinfection water, degrading trace metals, breaking down organic compounds, and eliminating inorganic contaminants.

2.2.1.1. Removal of trace metals

Because of serious health hazards caused by trace metals, including Pb, Cr, (Hg), and others, they have been successfully removed using heterogeneous photocatalysts (Farhan et al., 2023).

2.2.1.2. Hydrogen production

Hydrogen is considered a potential future fuel. While there are several techniques for generating hydrogen, hydrogen from water using visible light is especially prized as a renewable resource. It is a clean fuel that does not release CO_2 or other contaminants (Fatima et al., 2025).

2.2.1.3. Degradation of organics

A variety of organic compounds, including carboxylic acids, chlorinated aromatic compounds, and alcohols, are effectively degraded by using photocatalysis, producing harmless byproducts such as CO_2, simple mineral acids, and water (Akerdi & Bahrami, 2019)..

2.3. Photocatalytic Behavior of Fe_2O_3 Nanoparticles

Iron oxide exists in many stoichiometric and crystalline forms, including magnetite (Fe_3O_4), hematite (α-Fe_2O_3), wustite (FeO), and maghemite (γ-Fe_2O_3)(Mishra & Chun, 2015). Of these, α-Fe_2O_3 nanoparticles have received tremendous consideration due to their availability and nontoxic nature, with a narrow band gap (W. Huang et al., 2023). Hematite can capture light up to 600 nm and trap about 40 percent of solar energy (Valášková, Tokarský, Pavlovský, Prostějovský, & Kočí, 2019). Hematite is used in many different sectors such as pigments, gas sensors, dye degradation, optical devices, water purification, hydrogen production, and lithium-ion batteries (Kumar et al., 2022). Hematite nanoparticles can form different sizes and shapes, such as nanocubes, nanowires, and nanofibres (Abdulkadir, Abdallah, Jonnalagadda, & Martincigh, 2018). However, the photocatalytic efficiency of α-Fe_2O_3 is limited by low diffusion lengths of holes, low surface area, and high electron-hole recombination (Valášková et al., 2019). Therefore, numerous studies have concentrated on modifying α-Fe_2O_3 using various methods such as doping with different materials, altering the surface properties, creating composite structures, incorporating supporting materials, and forming heterostructures, as shown in Fig.2 (Hitam & Jalil, 2020; Khalaf et al., 2024).

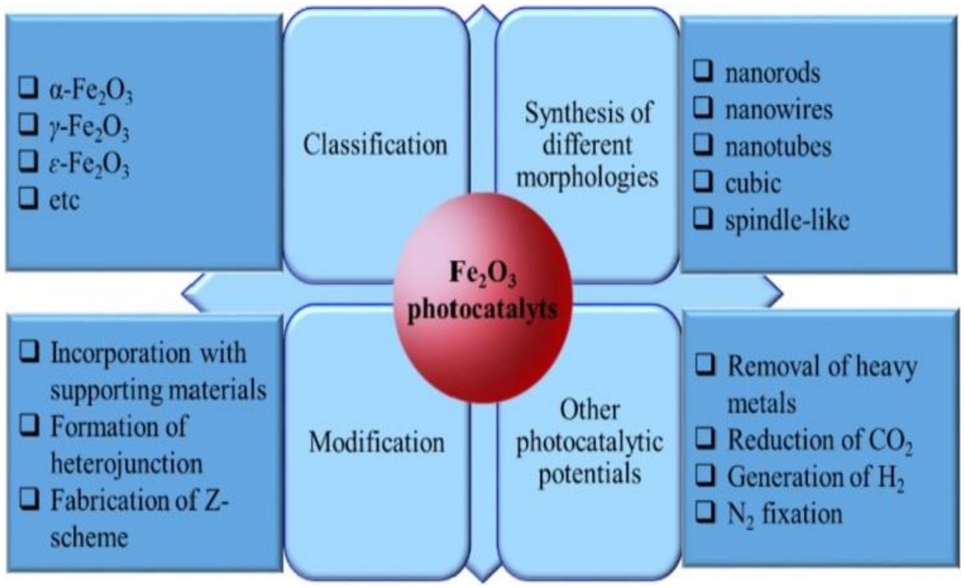

Figure 2: Fe_2O_3 Photocatalyst (Hitam & Jalil, 2020).

2.3.1. Modification of Fe_2O_3 as photocatalyst

Researchers have made several attempts to address the limitation of a single α-Fe_2O_3 using various techniques, such as surface modification, doping with different materials, the formation of heterostructures, and the preparation of composite materials (Hitam & Jalil, 2020). Among these approaches, the preparation of composite materials has been very effective in addressing the limitation of single hematite. Nanocomposite materials are composed of many phases and have at least one, two, or three dimensions in the nanoscale range (10^{-9} m)(Omanović-Mikličanin et al., 2020). Furthermore, composites efficiently harvest visible light, have higher charge separation capacity, improved resistance to photo-corrosion, and all contribute to their outstanding photocatalytic activity (Suresh et al., 2023).

The choice of photocatalytic materials relies on their valence and conduction band potentials, as well as their energy band gap. Depending on the type of semiconductor, various nanocomposites can be created, such as p-n, p-p, n-n, p-n-p, and n-p-n (Omanović-Mikličanin et al., 2020). One semiconductor photocatalyst with a compatible band potential is usually combined with another in composite systems. The photogenerated charge carriers can efficiently move between these semiconductor photocatalysts when they are exposed to the proper light sources, improving their overall photocatalytic activity as illustrated in Fig. 3 (Balapure, Dutta, & Ganesan, 2024).

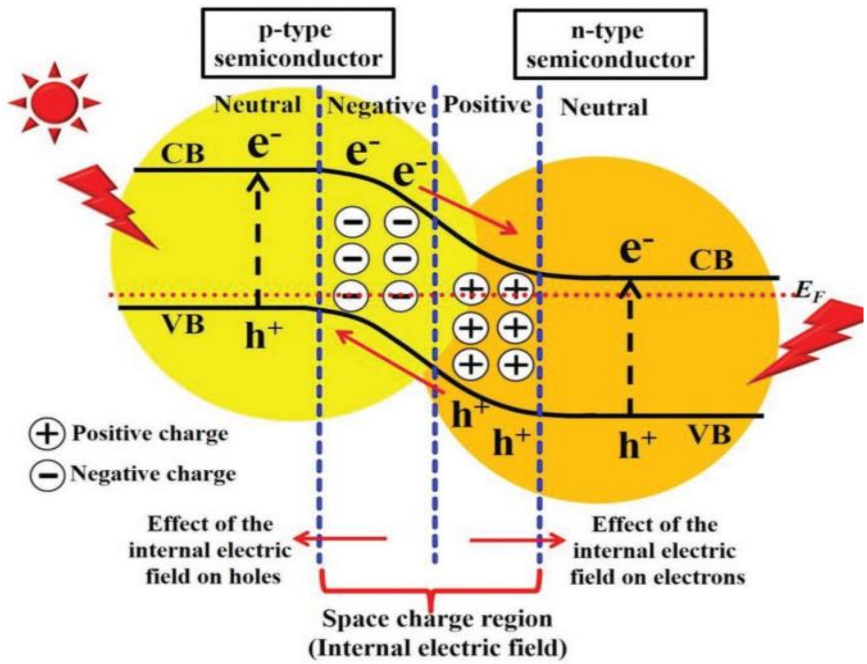

Figure 3: Mechanism of p–n heterojunction (Low et al., 2017)

Fe_2O_3 is one of the promising candidates among visible, recognizable photocatalysts. Fe_2O_3 is combined with other metal oxides to form composites in different applications. Fe_2O_3 photocatalysts have been combined with various materials, such as α-Fe_2O_3/ZnO (Xie et al., 2015), Fe_2O_3/TiO_2 (Moniz, Shevlin, An, Guo, & Tang, 2014), α-Fe_2O_3/activated carbon (Ranjithkumar, Sangeetha, & Vairam, 2014), α-Fe_2O_3/NiO (Devi et al., 2025), g-C_3N_4/α-Fe_2O_3 (L. Y. Huang, Zhang, Sun, & Cheng, 2014), O-g-C_3N_4/TiO_2/α-Fe_2O_3 (Aghababaei, Abdouss, Hosseini-Monfared, & Ghanbari, 2023), NiO/ZnO/Fe_2O_3 (Islam et al., 2022). Extensive research has been done on the synergistic combination of Fe_2O_3 and NiO to enhance photocatalytic properties under visible light. NiO is a p-type semiconductor and has a bandgap energy of 3.0-4.0 eV, has shown great promise for improving the photoactivity of Fe_2O_3 associated with its high separation of charge carriers, non-toxicity, and is an ideal option for practical applications in photocatalysis (Mou et al., 2022).

(Devi et al., 2025) synthesized α-Fe_2O_3/NiO composite (1:1, 2:1, and 1:2) via the co-precipitation method for the degradation of Rose Bengal dye. Among these, α-Fe_2O_3/NiO (2:1) showed a higher degradation of 94% in ninety) min. The reported high photocatalytic performance of α-Fe_2O_3/NiO (2:1) composite due to synergistic effects between α-Fe_2O_3 and NiO, retards the photoexcited charge carrier recombination, as illustrated in Figure (4).

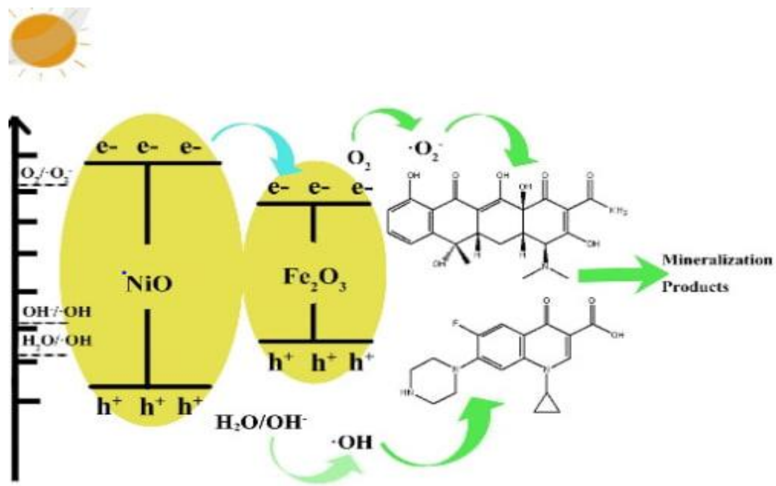

Figure 4: P-n heterojunction between NiO and Fe_2O_3 (Devi et al., 2025).

Recently, many carbons with variable chemical and physical properties have been created (Ayanda et al., 2024), such as activated carbon (AC) (Bukhari et al., 2024), carbon spheres (CSs) (Amel Boudjemaa et al., 2015), carbon nanotubes (CNTs) (Aslam et al., 2021), graphene (M. A. Ahmed & Mohamed, 2023), and carbon fibers (CFs) (B. Tahir, Tahir, Alraeesi, & Kumar, 2024) are widely recognized. These carbon materials have fascinating electrical conductivity, a large surface area, relative chemical inertness, high porosity, high stability, and environmentally sustainable materials (Baniamerian et al., 2021).

(Ismail et al., 2019) synthesized mesoporous CNT-α-Fe_2O_3 nanohybrids by the sol-gel technique. The synthesized mesoporous CNT-α-Fe_2O_3 efficiency was evaluated for degradation of Bismarck Brown R Dye. The degradation performance increased from 83% to 98% when CNT amounts increased from 0 to 50 percent. Removal of BBR dye using 50% CNT/α-Fe_2O_3 35 times higher than using single Fe_2O_3. The higher photocatalytic efficiency of mesoporous nanohybrids CNT-α-Fe_2O_3 than mesoporous α-Fe_2O_3 is due to the synergistic impact and successful separation of electron-hole pairs.

(Amel Boudjemaa et al., 2015) Synthesized iron oxide by the deposition precipitation technique, which is supported on CSs. This material's efficiency was evaluated for the production of hydrogen when exposed to visible light. Both the composition and the size of the iron oxide particles on CSs enhance electron-hole separation, which leads to an improved performance in the production of H_2.

(Yu et al., 2017) synthesized α-Fe_2O_3 /graphene composite by the hydrothermal method. The photodegradation of MB dye results indicated that (α-Fe_2O_3 /G) composites exhibited better photocatalytic activity than a single α-Fe_2O_3 due to a comprehensive light capture range and higher electron-hole separation rate.

Activated carbon (AC) has extensive applications across various fields for its low cost, porous structure, high surface area, and variable surface characteristics. Furthermore, AC enhanced separation of electron-hole by capturing the charge, providing adsorption sites, and improving capture of visible light (Zou et al., 2019). (Faheem et al., 2024) prepared γ-Fe_2O_3/AC by the co-precipitation method to degrade MB and (MO) dyes, and the 1:3 sample exhibited 94% photodegradation of MO dye at 180 min and 87% degradation of MB dye in 125 min. γ-Fe_2O_3/AC had high potential towards photodegradation of MO and MB attributed to the presence of carbon that helps to capture electrons in the CB of maghemite and retards them from recombining with holes in the VB of γ-Fe_2O_3.

2.4. Synthesis Methods of Nanocomposites

Nanocomposites can be synthesized by several methods. The most common are hydrothermal, sol-gel, and co-precipitation. Among these methods, co-precipitation is a cost-effective, straightforward, and common technique to achieve small particle size (Santoshi et al., 2024). Different authors used the co-precipitation method to prepare nanocomposites such as Fe_2O_3/NiO/C(Amel Boudjemaa et al., 2015), (Ismail et al., 2019),(Faheem et al., 2024),(Li et al., 2013), (Al-Alawy, Al-Abodi, & Kadhim, 2018), Fe_2O_3/NiO, Fe_2O_3/ZnO, (Usman et al., 2024), and (Patwa, Rohilla, & Rani, 2024).

2.5. Property of Methylene Blue (MB)

Methylene blue (MB) is a cationic and basic aromatic heterocyclic dye, as shown in Fig .5 (I. Khan et al., 2022). The methylene blue absorption spectrum has a strong peak at approximately 664 nm that gets smaller as the photodegradation occurs. The dye has many uses in many factory like food, textiles, medicine, pharmaceuticals, printing, painting, paper production, and dyeing (Zarei, Hasheminiasari, Masoudpanah, & Javadpour, 2022).

Methylene blue dye is harmful to humans and aquatic life. MB leads to many diseases like respiratory distress, gastrointestinal disorder, blindness, and mental instability (Shakoor & Nasar, 2017).

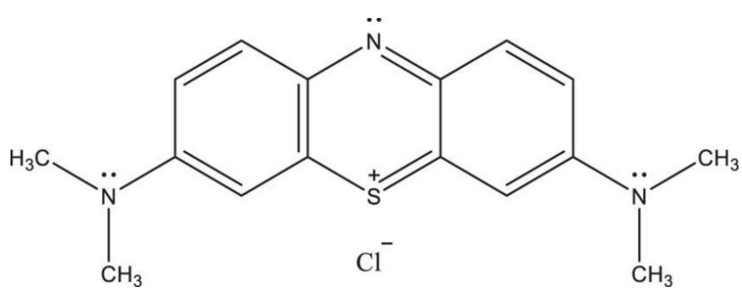

Figure 5:Structure of methylene blue (MB) dye (Oladoye, Ajiboye, Omotola, & Oyewola, 2022)

Several methods have been published to eliminate toxic dyes such as methylene blue from industrial wastewater streams. They are adsorption, biodegradation, and coagulation (Bashir et al., 2019). Nowadays, photocatalytic degradation of organic pollutants by single-component and multiple-component semiconductors has gained extensive attention due to inexpensive, eco-friendly, and easy treatment of wastewater containing hazardous pollutants. A single-component photocatalyst is presented in Fig.6 (Hanif et al., 2019). Fig.7 illustrates a multi-component photocatalyst system consisting of Fe_2O_3, graphene, and CuO (Nuengmatcha, Porrawatkul, Chanthai, Sricharoen, & Limchoowong, 2019).

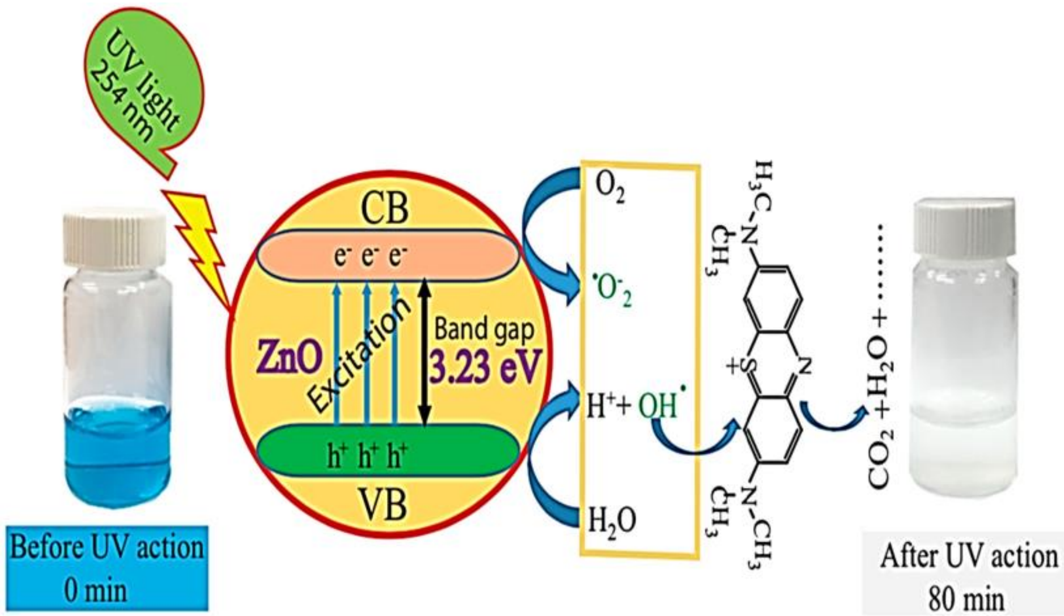

Figure 6: ZnO nanoparticles for methylene blue degradation (Hanif et al., 2019).

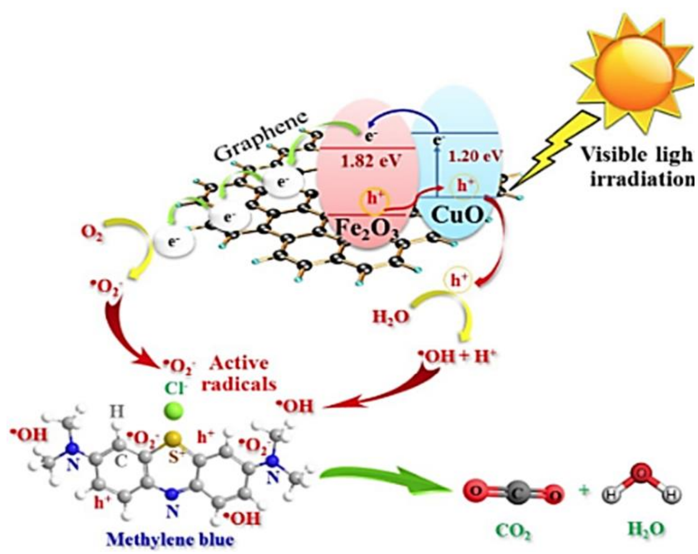

Figure 7: The Fe_2O_3/graphene/CuO nanocomposite photocatalytic mechanism

(Nuengmatcha et al., 2019)

2.6. Factors Affecting Photocatalytic Degradation of Methylene Blue

Photocatalytic activity might be affected by a variety of parameters such as pH, the dye concentration, and the presence of oxidants.

2.6.1. Dye concentration

A dye's initial concentration affects the rate of photodegradation. The photocatalysis rate is increased by increasing the concentration of (MB) because more MB molecules are available on the catalyst's surface. However, above a certain optimal concentration, further increases in MB lower photocatalytic performance due to decreased collisions between the dye and the $OH^{\bullet}$(M. Ahmed, El-Naggar, Aldalbahi, El-Newehy, & Menazea, 2020).

2.6.2. pH

Methylene blue (MB), which is a cationic dye, tends to adsorb more effectively onto a solution that carries a negative charge. In alkaline solutions, the photocatalyst has a negative charge, which helps it attract and hold onto positively charged dye. In contrast, in lower pH solutions, MB dye and H^+ ions compete for adsorption sites on the photocatalyst, resulting in a lower uptake of MB molecules (I. Khan et al., 2022).

2.6.3. Oxidants

The photodegradation efficiency of the catalyst is enhanced by the addition of oxidants. H_2O_2 increase $OH^{\bullet}$ formation and enhance the degradation of pollutants due to the retardation of photogenarated charge carriers (I. Khan et al., 2022).

2.6.4. Catalyst

The kind of catalyst employed and its concentration have a significant impact on the effectiveness of methylene blue (MB) photodegradation (Dehno Khalaji, 2022), as depicted in Table 1.

Table 1: Photocatalytic activity of various catalysts for degradation of MB

Photocatalyst	Crystal size (nm)	Catalyst dosage (mg)	Dye concentration (mg/l)	Degradation time (min)	Degradation efficiency (%)	Reference
α $-Fe_2O_3$	34.55	20	30	70	97	(Dehno Khalaji,

						2022)
NiO	21	40	5	120	84.9	(Gebreegziabher, Yicheneku, & Weldegebrieal, 2024)
Fe_2O_3/TiO_2	31.74	100	30	97.71	90	(Liu et al., 2024)
Fe_2O_3	35.38	10	10	120	78.68	(Goudjil, Dali, Zighmi, Mahcene, & Bencheikh, 2024)
CuO	13.4	50	20	210	97.67	(Nouren et al., 2024)

CHAPTER THREE

3. METHODS AND MATERIALS

3.1. Study Site Description

Synthesis of Fe_2O_3/NiO/C composite was conducted at Adama Science and Technology University (ASTU), Department of Applied Chemistry. XRD characterization of the synthesized nanocomposite was conducted at ASTU, Department of Material Science and Engineering. PL analysis was done in the Department of Applied Physics. FESEM-EDX analysis was carried out in India. UV-Vis spectrophotometer was used to analyze the photocatalytic activity was conducted at the Department of Material Science and Engineering. FTIR analysis was conducted at Addis Ababa Science and Technology University.

3.2. Chemicals and Reagents

The chemicals, reagents, and solvents used during this study include sodium hydroxide (NaOH) (98%) as a precipitating agent; potassium hydroxide (KOH) to activate the SCGs; hydrochloric acid (HCl) and ethanol (96%) for washing; methylene blue dye as a sample pollutant; $Ni(NO_3)_2.6H_2O$ (98%) from Loba Chemie Pvt. Ltd., India, as a source of Ni^{2+}; and $Fe(NO_3)_3.9H_2O$ (98%) from Loba Chemie Pvt. Ltd., India, as a source of Fe^{3+}. All the chemicals and reagents used were analytical grade, and used without any treatment.

3.3. Apparatus and Instruments

Apparatus used for this work were different-sized beakers, a conical flask, measuring cylinder, Whitman No.1 filter paper, magnetic stirrer, crucible, spatula, pH meter, centrifuge, and aluminum foil. The instruments used for this study were XRD (Model XRD-7000, Company Japan), UV-Vis DRS (UV-Vis DRS, ElicoSL-150 spectrophotometer), FESEM (FE-SEM, ZEISS SIGMA VP, Germany), FTIR (IS50 ABX Thermoscientific, USA), and PL (Cary Eclipse, S/N: MY18490002, Agilent technologies) spectroscopies.

3.4. Methods

3.4.1. Preparation of carbon

Spent coffee grounds from the ASTU student cafe were collected and washed using distilled water. The SCGs were then dried overnight at 80 ℃. 30 g of SCGs was soaked in 250 mL of 3M KOH for 6 hours and then dried at 105 ℃ for 12 hours. Pyrolysis was then carried out at 600 ℃ for 2 hours. Then, the resulting carbonized powder was washed with 100 ml of 1 M HCl, followed by distilled water. Finally, drying was carried out at 80 °C overnight. This approach was modified from previously described methods for preparing activated carbon from biomass waste materials (L. Yao, Leng, Lan, Chen, & Jiang, 2022).

3.4.2. Synthesis of Fe_2O_3/NiO composite

The Fe_2O_3/NiO composite was synthesized using the co-precipitation method (Taufiq et al., 2020). In this method, 100 mL of (0.2M, 0.1M, and 0.2M) $Fe(NO_3)_3.9H_2O$ and 100 mL of (0.2M, 0.2M, and 0.1M) ($Ni(NO_3)_2.6H_2O$) were combined, corresponding to 1:1, 1:2, and 2:1 molar ratio, respectively. The obtained mixtures were mixed at 25 °C for 4 hours. After the stirring time finished, the formed solution pH was checked and adjusted to 10 by adding a small quantity of 2M NaOH solution. Then, the obtained suspension was stirred additionally for 30 min. The obtained solution was allowed to stay in a refrigerator overnight. Following this, the precipitated mixture was filtered by Whitman filter paper. The collected precipitates were washed and then dried for 2 hours at 80°C. Finally, the dried precipitate was crushed and calcined at 500°C for 3 hours using a muffle furnace.

3.4.3. Synthesize of Fe_2O_3/NiO/C nanocomposite

The Fe_2O_3/NiO/C composite was synthesized by using the co-precipitation method (Baniamerian et al., 2021). In detail, 100 mL of (0.2 M, 0.1 M, and 0.2M) Fe $(NO_3)_3.9H_2O$ was combined with 100 mL of (0.2M, 0.2M, and 0.1 M) Ni $(NO_3)_2.6H_2O$, corresponding to 1:1, 1:2, and 2:1 molar ratio, respectively with stirring the mixtures at 25 °C for 30 min. Consequently, 50 mL of a carbon suspension (0.2 g of carbon in water) was added and named as (1:1)C, (1:2)C, and (2:1)C, respectively. The mixtures were mixed for 4 hours. Then, the pH of solutions was checked and adjusted to pH 10 through dropwise addition of 2M NaOH solution. The resulting suspension was stirred for 30 min. The obtained mixture was stored in a refrigerator overnight. Following this, the precipitated mixture was filtered, collected, and the collected precipitates were washed and then dried for 2 hours at 80°C. Finally, the obtained product was crushed and calcined at 500°C for 3 hours using an amuffle furnace. Additionally, the flowchart for this synthesis method is presented in Fig.8.

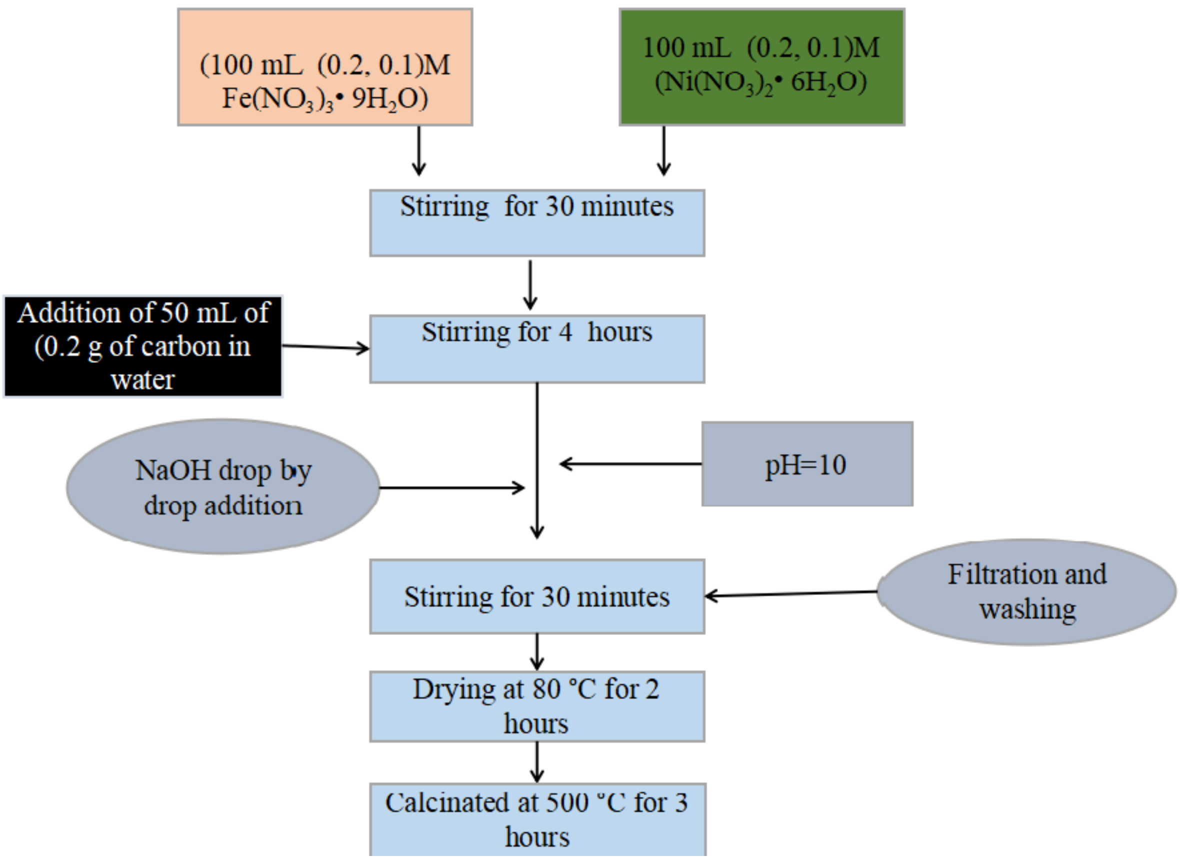

Figure 8: Flowchart for synthesis of Fe_2O_3/NiO/C nanocomposite using co-precipitation metod

3.4.4. Characterization of Fe_2O_3/NiO/C composite

The crystalline structure of the synthesized composites was analyzed by XRD. The synthesized nanocomposite morphology was characterized using FESEM, and elemental composition was analyzed using EDX. The energy band gap of the prepared nanocomposites was analyzed by UV-Vis DRS. The electron-hole recombination rate of synthesized nanocomposites was analyzed using PL spectroscopy. The functional groups and chemical bonds present in synthesized nanocomposites were analyzed by FTIR spectroscopy.

3.5. Photocatalytic Study

3.5.1. Photocatalytic experiment

The synthesized composite performance was assessed for the degradation of MB. 10 mg of the synthesized sample was mixed with 100 mL of a 30 mg/L MB solution in a beaker. Then the solution was mixed for 30 min in the absence of light to establish adsorption-desorption equilibrium. The suspension was then irradiated with a tungsten halogen lamp (150 W). At 5 min time intervals, 4 mL aliquots were taken, followed by centrifugation and filtration. The solution absorbance in the filtrate was measured by a UV-Vis spectrophotometer (UV-3600Plus Series). Degradation efficiency (D) was obtained by using the following formula (Goudjil et al., 2024).

$$\% \mathbf{D} = \left(\frac{\mathbf{A0-At}}{\mathbf{A0}}\right)*100\% \quad \text{…………….. ……………………………………………….1}$$

Where: - A_0 represents the initial absorption of dye; A_t is the absorption of dye at t time

CHAPTER FOUR

4. RESULTS AND DISCUSSION

4.1. Characterization of Fe_2O_3/NiO/C Nanocomposite

4.1.1. X-Ray diffractometer (XRD) analysis

The XRD pattern of the prepared Fe_2O_3/NiO/C composite was investigated to verify the purity, crystallinity, crystal structure, and crystallite size. The α-Fe_2O_3/NiO/C and α-Fe_2O_3/NiO nanocomposite composites XRD patterns with different molar ratio were illustrated in Fig. 9. The findings indicated that peaks appeared at 2θ angles of 30.38°, 35.77°, 54.07°, 57.55°, and 63.03°, representing the (220), (110), (422), (511), and (440) crystallographic planes and match well with the ICSD Card No.6075–009-98. This confirms the development of hexagonal crystalline α-Fe_2O_3 (Goudjil et al., 2024). Peaks were appeared at 2θ angles of 37.45 and 43.28° representing the (111) and (200) planes, the typical peaks of NiO and match well with the (JCPD 00-047-1049 NiO) (Mummoorthi, Shajahan, Abu Haija, Mahalingam, & Rajendran, 2022). The peak intensity slightly differs with composition. Notably, the carbon-containing samples, such as (1:1)C, (1:2)C, and (2:1)C, show similar peak positions to their analogous non-carbon samples but exhibit slight broadening and reduced intensities. It could be a result of the amorphous nature of carbon, which can coat the crystalline particles and reduce the overall diffraction intensity. However, no noticeable peak related to carbon was seen. This could be the low amount of carbon and its amorphous nature (Ermanda, Lubis, & Ramli, 2021). The average crystallite size of the prepared nanocomposites was calculated by the Scherrer equation (Holzwarth & Gibson, 2011).

$$D=\frac{k\lambda}{\beta\cos\theta} \qquad \text{……………… ………………………………………..2}$$

where k represents a constant 0.9, λ represents the wavelength (0.15406 nm), β stands for the full width at half Maximum (FWHM) of the diffraction line, and θ corresponds to the diffraction angle

According to the data presented in Table 2, the α-Fe_2O_3/NiO composite had the lowest crystallite size, which increased after the inclusion of carbon (Table 2). This evidence was confirmed by the incorporation of carbon into the surface of the α-Fe_2O_3/NiO composite (Lubis, Ramli, & Ermanda, 2020). Higher crystallite sizes belonged to (1:1) C (19.98 nm) and 2:1 (19.98 nm). Smaller crystallite sizes were 1:2 (10.40 nm) and (1:2) C (13.22).

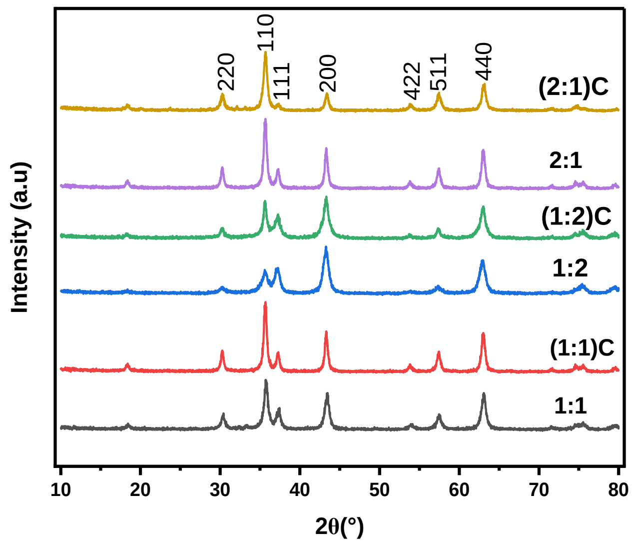

Figure 9: XRD patterns of α-Fe_2O_3/NiO and α-Fe_2O_3/NiO/C nanocomposites**.**

Table 2: Calculated crystallite size of synthesized composites

Sample	2 θ (Degree)	β (Radian)	D (nm)	Average crystallite size (nm)
1:1	35.7719	0.00933	15.61808	15.03
	43.3902	0.01092	13.66478	
	63.0309	0.01027	15.82967	
(1:1)C	35.6697	0.00768	18.97128	19.89
	43.3106	0.00725	20.56711	
	62.9871	0.00807	20.14431	

1:2	37.156	0.01466	9.97755	10.40
	43.262	0.0146	10.21546	
	62.8724	0.01474	11.02289	
(1:2)C	35.6448	0.01004	14.51284	13.22
	43.2867	0.01274	11.7082	
	62.9294	0.01208	13.45935	
2:1	35.6697	0.00768	18.97128	19.89
	43.3106	0.00725	20.56711	
	62.9871	0.00807	20.14431	
(2:1)C	35.6851	0.0095	15.33032	15.86
	57.4272	0.01054	14.99712	
	63.0533	0.00942	17.25934	

4.1.2. Fourier transform infrared (FTIR) analysis

The functional groups of the synthesized nanocomposites were examined by FTIR spectra that range from 500 to 4000 cm^{-1}. The FTIR result of α-Fe_2O_3/NiO nanocomposites with molar ratio of 1:2 (α-Fe_2O_3/NiO) and α-Fe_2O_3/NiO/C (1:2)C are shown in Fig. 10. The bands seen at 538 and 542 cm^{-1} in the (1:2)C and 1:2 samples are attributed to Fe-O and Ni-O bond stretching of α-Fe_2O_3 and NiO for the α-Fe_2O_3/NiO/C (1:2)C and 1:2 (α-Fe_2O_3/NiO), respectively (Shah, 2023). The C-O stretch bond of ether groups was observed at 1216 cm^{-1}, while the C=C stretch of aromatic groups was observed at 1368 cm^{-1}. Those peaks suggested that the prepared carbon from SCGs developed organic compounds, causing these functional groups to appear in the (1:2)C sample (Pagalan Jr et al., 2020).

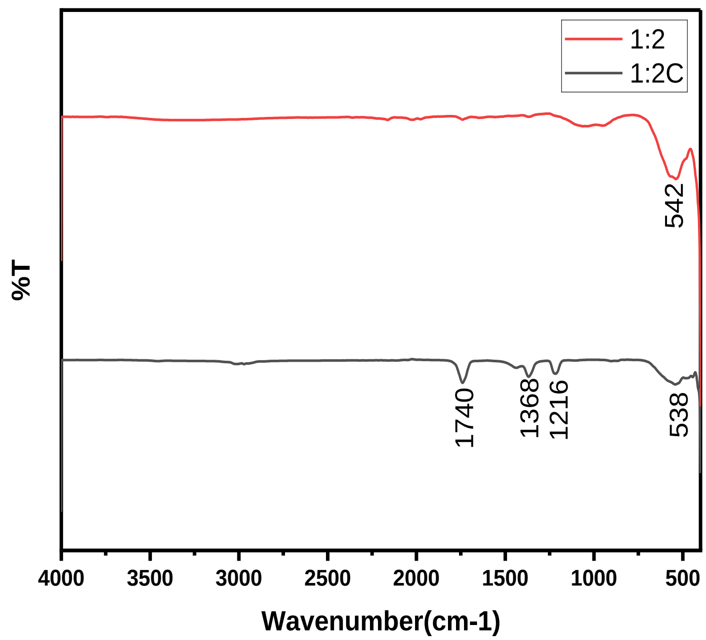

Figure 10: FTIR spectra of α-Fe_2O_3/NiO (1:2), and α-Fe_2O_3/NiO/C (1:2)C composites

4.1.3. Photoluminescence (PL) analysis

PL spectroscopy was utilized to analyze the recombination rate of charge carriers (Baniamerian et al., 2021). Fig. 11 shows the PL spectra of α-Fe_2O_3/NiO and α-Fe_2O_3/NiO/C nanocomposites with 300 nm excitation. From Fig.11, PL spectra of the (1:2)C composite exhibited the lowest PL peak intensity among the synthesized composites, suggesting a lower charge carrier recombination (Baniamerian et al., 2021). Furthermore, a PL intensity of Fe_2O_3/NiO (1:2) is higher than that of (1:2)C. The lower PL intensity of the (1:2)C composite is because the incorporation of carbon retards the recombination of charge carriers (Han et al., 2024). The photocatalytic performance of the (1:2)C nanocomposite was improved by the reduction in recombination of charge carriers.

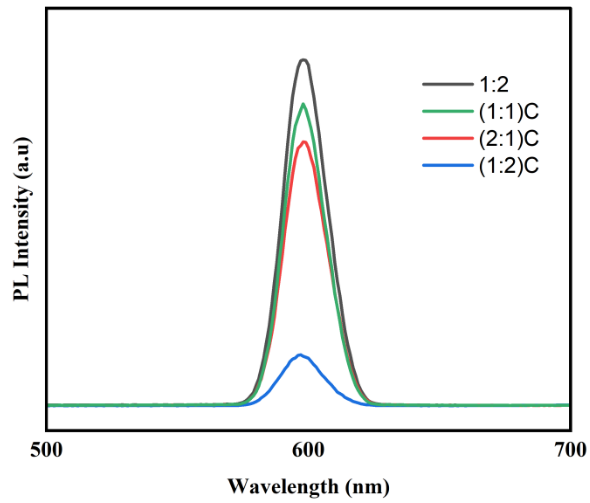

Figure 11: PL spectra of synthesized composites

4.1.4. Ultraviolet -visible diffuse reflectance spectroscopy (UV-Vis DRS)

The synthesized nanocomposite energy band gap was estimated by using UV-Vis DRS and estimated by the Tauc formula:

$(\alpha hv)^n = k(hv-E_g)$……………………………………………………………………..3

Where h represent the Planck constant; α mean the absorbance coefficient, which is similar to the kubelka- muck function F(R); n correspond the type band gap transition (n = 2 for direct transitions and n = 1/2 for indirect ones); k stand for the absorption constant; v represent the light frequency; and E_g means the energy band gap. The synthesized composite band gap energy was estimated by extrapolating $(\alpha hv)^2$ on the energy (hv), as illustrate Fig.12. The energy band gap of the synthesized composites was 2.44, 2.44, 2.47, and 2.43 eV for the molar ratios of 1:2, (1:1)C, (1:2)C, and (2:1)C composite, respectively. From the Fig.12 (A-D) information, the energy band gap of the synthesized composites shows approximately similar values, and the lower band gap of all synthesized nanocomposites confirmed their performance in exposure to visible light (Baniamerian et al., 2021).

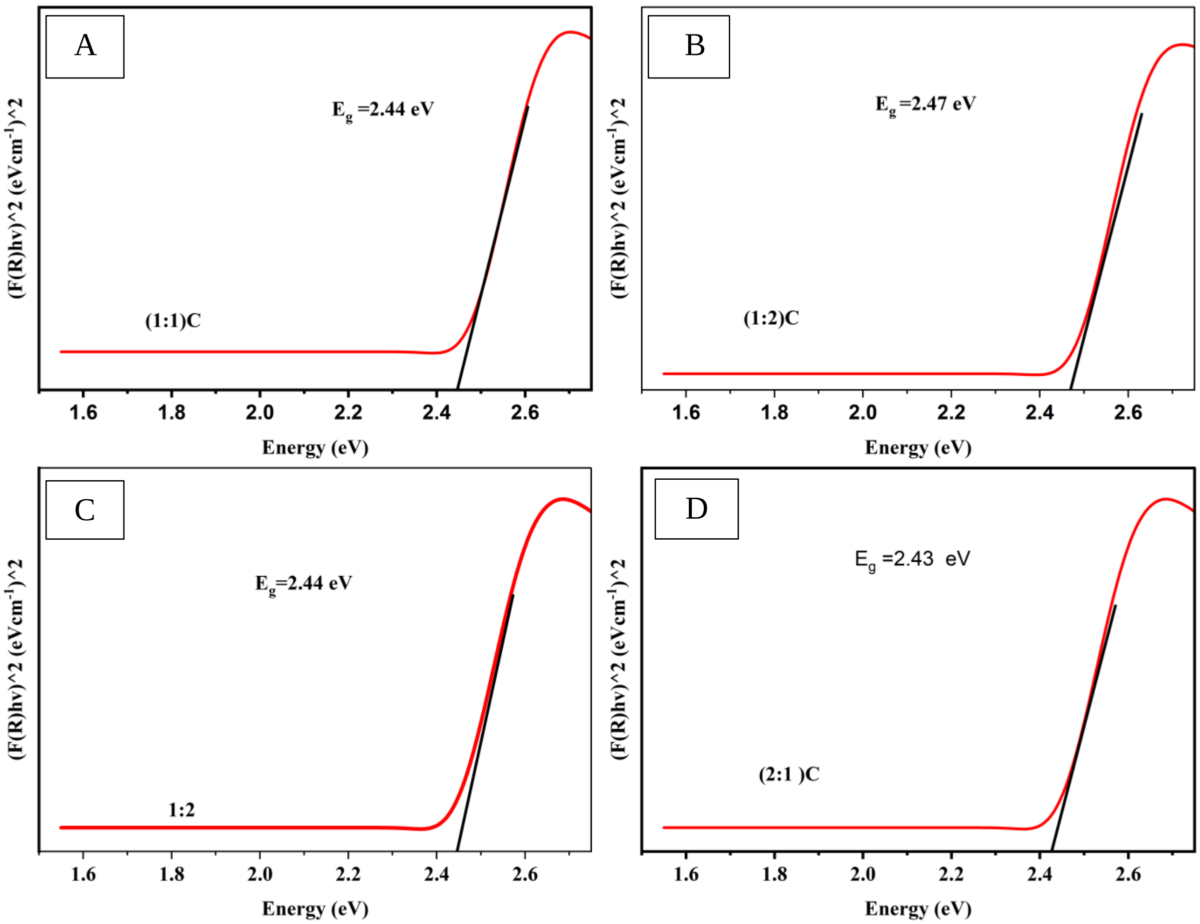

Figure 12: Tauc plots for bandgap energy estimation for synthesized nanocomposites: (A) (1:1)C, (B) (1:2)C; (C) 1:2; (D) (2:1)C

4.1.5. Field emission scanning electron microscopy (FESEM)

The surface morphology of (1:2)C sample was confirmed by FESEM, and the result presented in Fig. 13(A) shows the (1:2)C composite FESEM images. The image shows particles assembling into a granular structure with irregular morphology and a porous texture. This granular structure is due to the agglomeration in some regions, which may have resulted from the synthesis or the calcination process (Alhashem, Awada, Ahmed, & Farha, 2021; Baniamerian et al., 2021). The irregular morphology may be due to the variation of particle size as shown in Fig.13(I) (Alhashem et al., 2021). The energy dispersive X-ray spectroscopy (EDX) analysis of (1:2)C composite was shown in Fig.13(H), confirming that Fe, Ni, O, and C elements with atomic percent of 24.17, 18.90, 48.25, and, 6.72%, respectively, which proves the existence of Fe_2O_3, NiO, and C in the composite. The EDX also confirms the sulphur (S) element with an atomic percent of 1.96%, which might be due to the prepared carbon from spent coffee grounds containing trace amounts of sulphur (Figueroa Campos et al., 2021). The distribution of an element was shown in Fig.13(C–G), and the average particle distribution was found to be 32.7nm, as presented in Fig.13(I).

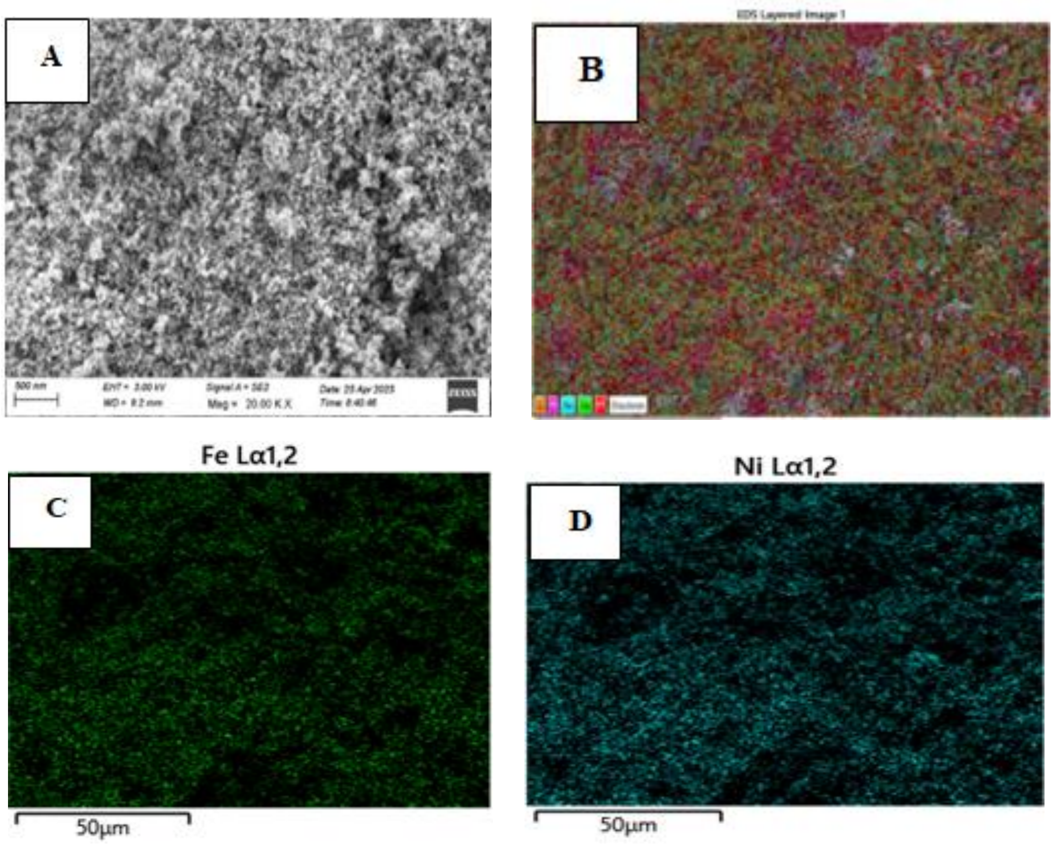

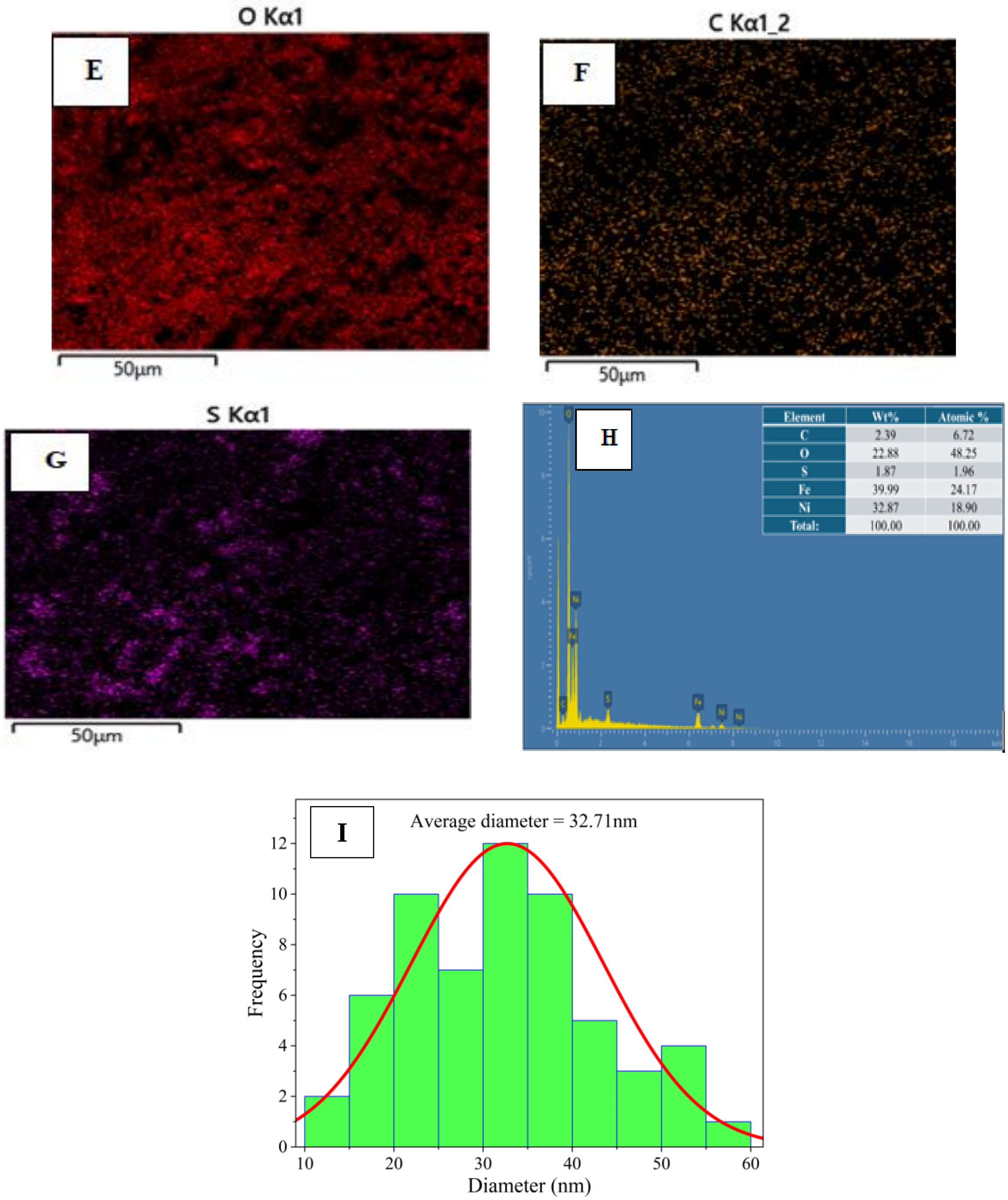

Figure 13: The morphological and compositional analysis result of (1:2)C composite: (A) FESEM image; (B) EDS layered image; Fig 13 .C- G elemental mapping of Fe, Ni, O, C, and S, respectively (H) EDX spectrum of (1:2) C composite; (I) average diameter distribution of (1:2)C composite

4.2. Photocatalytic Activity Test

The degradation performance of the synthesized composites was tested for the degradation of MB. After stirring the MB solution with the catalyst for 30 minutes in the absence of light to achieve adsorption-desorption equilibrium, the experiments were conducted under visible light (Hitkari, Sandhya, Gajanan, Shrivash, & Deepak, 2018). However, the absorption peak of MB was broad and shifted to 614 nm due to its high concentration (30 mg/L and 50 mg/L), which is consistence with the previous study (Hitkari et al., 2018). To select the best materials, 1:2 (1:1)C, (1:2)C, and (2:1)C samples were assessed for the photodegradation of MB with a dye concentration of 30 mg/L, 15 mg catalyst dosage, pH 9, and irradiation time of 15 minutes. Table 4 shows the degradation efficiency of samples 1:2, (1:1)C, (1:2)C, and (2:1)C were 74.44%, 80.23%, 91.65%, and 87.22%, respectively. Among these, the (1:2)C composite indicated the highest degradation efficiency as shown in Fig.14(A) and supported by Table 3. The decrease in absorption peaks gradually showed that the photodegradation reaction occurred. After 30 minutes in the dark, the removal efficiency of Fe_2O_3/NiO (1:2) and Fe_2O_3/NiO/C (1:2)C was assessed. As shown in Fig. 14(B) and supported by Table 3, the degradation efficiency of the Fe_2O_3/NiO/C (1:2)C composite was greater than that of the Fe_2O_3/NiO (1:2) sample. The improved performance could be the enhanced adsorption capability caused by the addition of carbon into the composite. Furthermore, in comparison of the degradation efficiency of 1:2 and (1: 2)C, the (1:2)C composite exhibited greater degradation efficiency because of the contribution of carbon in electrons capture and decrease of recombination with holes (Faheem et al., 2024), and the increased dye adsorption, allows more MB molecules to attach to the surface of catalyst, which offers many active sites for the occurrence of photocatalytic (Baniamerian et al., 2021). As a result, further optimization was done on (1:2)C composite with varying conditions, including pH (5 and 9), dosage of catalyst (5 mg, and 10 mg), (30 mg/L and 50 mg/L) MB concentration, and irradiation times (5-30 minutes).

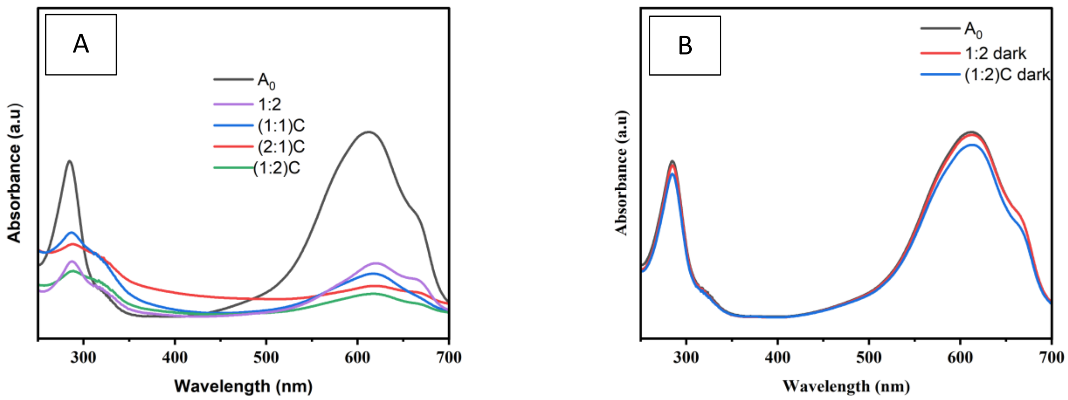

Figure 14: UV-visible spectra of MB with catalysts of: (A)1:2, (1:1)C, (2:1)C; (B) (1:2) dark an(1:2)C dark

Table 3: Degradation efficiency of synthesized composites

Sample	pH	Catalyst dosage (mg)	Time (min)	Degradation efficiency (%)
1:2	9	15	15	74.44
(1:1)C	9	15	15	80.23
(2:1)C	9	15	15	87.22
(1:2)C	9	15	15	91.65
1:2 dark	9	15	15	1.5
(1:2) C dark	9	15	15	7.32

4.2.1. Parameter optimization

4.2.1.1. Effects of catalyst dosage

Catalyst dosage is an effective parameter in the removal of organic contaminants (Dehno Khalaji, 2022). The photodegradation of MB was evaluated using 5 mg and 10 mg (1:2)C composite at constant pH 9 and dye concentration (30 mg/L). As illustrated in Table 4, the 10 mg catalyst dosage exhibited higher MB degradation efficiency due to the increased numbers of active sites at the photocatalyst surface, which enhances the formation of O_2• and HO•, which can degrade the MB through a redox reaction (Dehno Khalaji, 2022). Furthermore, the photocatalytic removal of MB kinetics was analyzed using first-order pseudo kinetics as presented in Fig.15 (Goudjil et al., 2024).

$$ln\left(\frac{A}{A0}\right) = -kt \qquad (4)$$

Where: A_0 represents the initial absorbance of MB, A_t absorbance of MB at t time

For the photodegradation of MB, the measured rate constants are 0.065 and 0.093 min^{-1} for (1:2)C composite with 5 and 10 mg catalyst dosage, respectively. From Fig.15, it is observed 10 mg catalyst dosage showed a higher photodegradation performance of MB than a 5 mg catalyst dosage of (1:2)C composite.

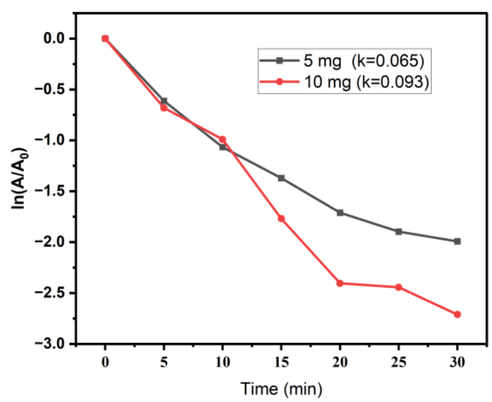

Figure 15: Pseudo first-order kinetics for MB degradation using 5 mg and 10 mg of (1:2)C composite

4.2.1.2. Effects of contact time

The impacts of contact duration for the elimination of MB by (1:2)C composite were conducted at 5-30 minutes at a steady MB concentration (30 mg/L), pH 9, and catalyst dosages of 5 mg and 10 mg. Fig. 16(A-B) and Table 4 show the impact of contact duration on the Uv-vis absorption spectrum and the photodegradation efficiency of MB, respectively. The maximum photodegradation of the MB was 86.37% for 5 mg and 93.35% for 10 mg after 30 minutes of irradiation. The outcomes revealed that MB photodegradation increased with increasing contact time. The decrease in the absorption spectra might be the reduction of the MB chromophore (I. Khan et al., 2022).

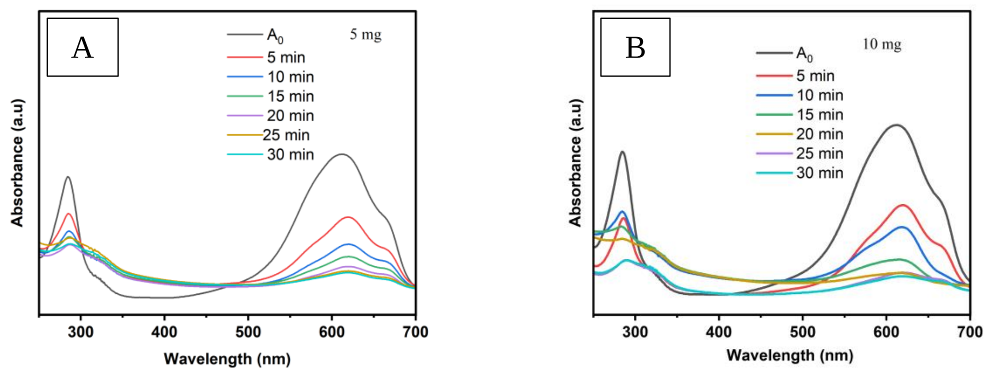

Figure 16: UV-visible spectra of MB with catalysts of (1:2)C:(A) 5 mg; (B) 10 mg

Table 4: Effects of contact time on photodegradation of MB with catalysts of (1:2)C 5 mg and 10 mg

Sample	Catalyst dosage (mg)	Time (min)	Degradation efficiency (%)
(1:2)C	5	10	65.58
		20	81.94
		30	86.37
	10	10	62.86
		20	90.97
		30	93.35

4.2.1.3. Effects of concentration of MB

The impacts of the concentration of MB were evaluated using 30mg/L and 50 mg/L at a steady pH of 9 with a 10 mg (1:2) C composite. From the obtained result in our study, when the initial concentrations of MB were 30 mg/L and 50 mg/L, the degradation performance of MB on the surface of (1:2) C composite decreased from 93.35% to 84.2% after 30 minutes of irradiation, respectively, as shown in Fig.17(A-B) and supported by Table.5. When, the concentration of dye increase; the speed of discoloration decreases. This result resembles the previous investigation (Dehno Khalaji, 2022).

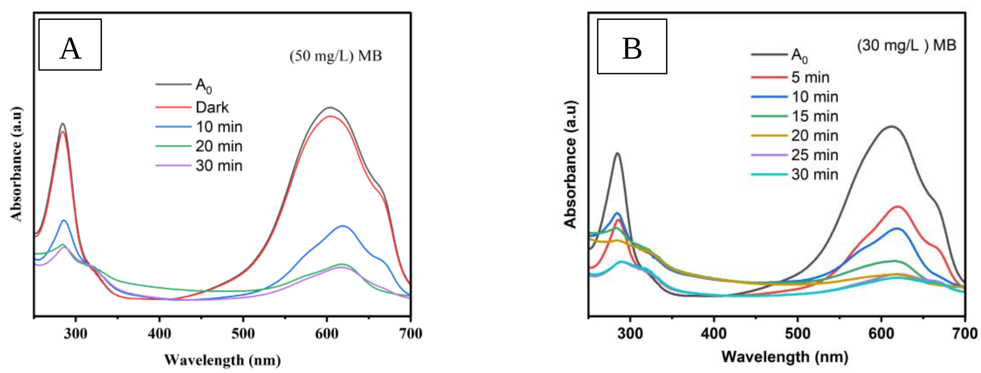

Figure 17: UV-visible spectra of MB with: (A) 30 mg/L; (B) 50mg/L concentrations of MB

Table 5: Effects of MB concentration on its degradation using 1:2)C composite

Sample	MB concentration (mg/L)	Time (min)	Degradation efficiency (%)
(1:2)C	30	10	62.86
		20	90.97
		30	93.35
	50	10	62.4
		20	82.6

		30	84.2

4.2.1.4 . Effects of pH

The effects of pH were studied using a pH of 5, 9, and 30 mg/L MB concentration, and 10 mg of (1:2)C. The results showed the photodegradation efficiency of (1:2)C composite at pH 5 was only 8.12%, while at pH 9 it increased significantly to 93.35% after 30 minutes of irradiation, as shown in the Table.6 supported by Fig.18(A-B), in the acidic medium (pH 5), the lower degradation efficiency might be the increased concentration of H^+ on the surface of (1:2)C composite competing with the cationic MB dye, which reduces the adsorption of the MB molecules on the surface of the photocatalyst (I. Khan et al., 2022). However, in the basic medium (pH 9), the degradation efficiency was higher due to increased electrostatic attraction between the (1:2)C composite and the MB molecules (Dehno Khalaji, 2022).

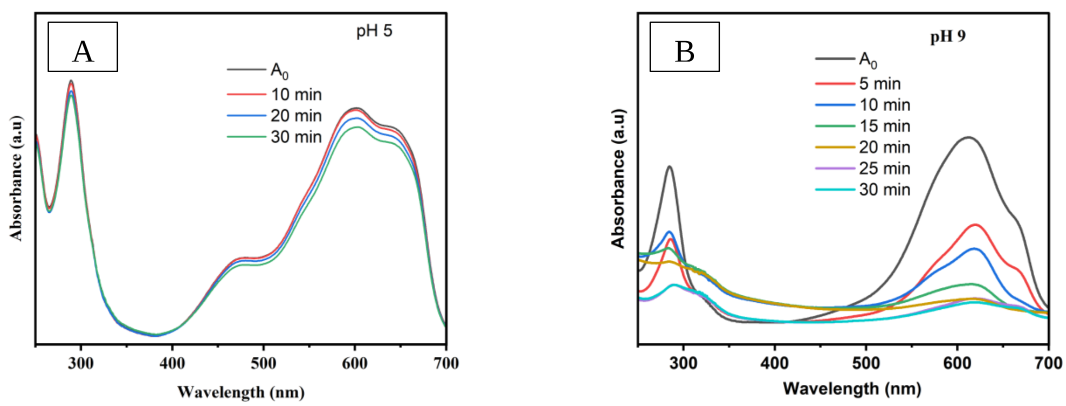

Figure 18: UV-visible spectra of MB with pH of: (A) 5; (B) 9

Table 6: Effects of pH on photodegradation of MB using (1:2)C composite

Sample	pH	Time (min)	Degradation efficiency (%)
		10	0.98

(1:2)C	5	20	4.34
		30	8.12
	9	10	62.86
		20	82.96
		30	93.35

5. CONCLUSION AND RECOMMENDATIONS

5.1. Conclusion

This study concentrated on synthesizing and characterizing Fe_2O_3/NiO/C composites using the co-precipitation method. Fe_2O_3/NiO/C composites were synthesized from precursor salt, Ni $(NO_3)_2.6H_2O$, Fe $(NO_3)_3.9H_2O$, and spent coffee ground-derived carbon with in (1:1)C, (1:2)C, and (2:1)C molar ratio. The synthesized materials were characterized by FESEM-EDX, FTIR, PL, XRD, and UV-Vis DRS. XRD was utilized to study crystallinity, crystallite size, and Crystal structure. The UV-Vis DRS result shows the estimated energy band gap was determined to be 2.44, 2.47, 2.43 eV for (1:1)C, (1:2)C, (2:1)C ration composite, respectively. In addition, the synthesized Fe_2O_3/NiO/C (1:2)C composite exhibited the highest efficiency for degrading MB dye in aqueous solution due to the lower charge carrier recombination compared with the (1:1)C and (2:1)C composite. Furthermore, Fe_2O_3/NiO/C (1:2)C showed higher degradation efficiency compared to Fe_2O_3/NiO (1:2) due to the addition of carbon lowers the recombination of electron-hole pairs. The maximum degradation efficiency of MB was 93.35% by using a 10 mg Fe_2O_3/NiO/C (1:2)C composite, at pH 9, 30 mg/L MB concentration, and 30 min irradiation time in a visible light source.

5.2. Recommendations

Future studies should concentrate on the application of Fe_2O_3/NiO/C (1:2)C as a photocatalyst at industrial levels to assess its practicality in real wastewater treatment. Also, future studies should investigate the reusability and long-term stability of the reported photocatalyst. We recommend further studies on the photocatalytic potential of the reported catalyst against pharmaceuticals, other dyes, and pesticides. Furthermore, we recommend that future studies utilize electron spin resonance (ESR) spectroscopy and reactive species taping experiments to determine the roles of $OH^{\bullet}$, $O_2^{\bullet}$, and h^+. ESR spectroscopy using DMPO as a spin-trapping agent could help confirm the formation of DMPO-$^{\bullet}OH$ and DMPO-$^{\bullet}O_2^-$ adducts during photocatalysis that play a significant role in its photocatalytic activities.

REFERENCES

Abdulkadir, I., Abdallah, H. M., Jonnalagadda, S. B., & Martincigh, B. S. (2018). The effect of synthesis method on the structure, and magnetic and photocatalytic properties of hematite (α-Fe_2O_3) nanoparticles. *South African Journal of Chemistry, 71*, 68-78.

Aghababaei, N., Abdouss, M., Hosseini-Monfared, H., & Ghanbari, F. (2023). Enhanced photo-degradation of diclofenac using a new and effective composite (Og-C3N4/TiO2/α-Fe_2O_3): degradation pathway, toxicity evaluation and application for real matrix. *Journal of Environmental Chemical Engineering, 11*(5), 110477.

Ahmed, M., El-Naggar, M. E., Aldalbahi, A., El-Newehy, M. H., & Menazea, A. (2020). Methylene blue degradation under visible light of metallic nanoparticles scattered into graphene oxide using laser ablation technique in aqueous solutions. *Journal of Molecular Liquids, 315*, 113794.

Ahmed, M. A., & Mohamed, A. A. (2023). Recent progress in semiconductor/graphene photocatalysts: synthesis, photocatalytic applications, and challenges. *RSC Advances, 13*(1), 421-439.

Akerdi, A. G., & Bahrami, S. H. (2019). Application of heterogeneous nano-semiconductors for photocatalytic advanced oxidation of organic compounds: A review. *Journal of Environmental Chemical Engineering, 7*(5), 103283.

Al-Alawy, A. F., Al-Abodi, E. E., & Kadhim, R. M. (2018). Synthesis and characterization of magnetic iron oxide nanoparticles by co-precipitation method at different conditions. *Journal of Engineering, 24*(10), 60-72.

Alegbe, E. O., & Uthman, T. O. (2024). A review of history, properties, classification, applications and challenges of natural and synthetic dyes. *Heliyon*.

Alhashem, Z., Awada, C., Ahmed, F., & Farha, A. H. (2021). Structural and magnetic properties study of Fe2O3/NiO/Ni2FeO4 nanocomposites. *Crystals, 11*(6), 613.

Alshehri, M., Al-Marzouki, F., Alshehrie, A., & Hafez, M. (2018). Synthesis, characterization and band alignment characteristics of NiO/SnO2 bulk heterojunction nanoarchitecture for promising photocatalysis applications. *Journal of Alloys and Compounds, 757*, 161-168.

Antonopoulou, M. (2022). Homogeneous and heterogeneous photocatalysis for the treatment of pharmaceutical industry wastewaters: A review. *Toxics, 10*(9), 539.

Aslam, M. M.-A., Kuo, H.-W., Den, W., Usman, M., Sultan, M., & Ashraf, H. (2021). Functionalized carbon nanotubes (CNTs) for water and wastewater treatment: preparation to application. *Sustainability, 13*(10), 5717.

Ayanda, O. S., Mmuoegbulam, A. O., Okezie, O., Durumin Iya, N. I., Mohammed, S. a. E., James, P. H., . . . Yahaya, S. M. (2024). Recent progress in carbon-based nanomaterials: critical review. *Journal of Nanoparticle Research, 26*(5), 106.

Balapure, A., Dutta, J. R., & Ganesan, R. (2024). Recent advances in semiconductor heterojunctions: a detailed review of the fundamentals of photocatalysis, charge transfer mechanism and materials. *RSC Applied Interfaces, 1*(1), 43-69.

Baniamerian, H., Teimoori, M., & Saberi, M. (2021). Fe2O3/TiO2/activated carbon nanocomposite with synergistic effect of adsorption and photocatalysis. *Chemical Engineering & Technology, 44*(1), 130-139.

Bashir, A., Malik, L. A., Ahad, S., Manzoor, T., Bhat, M. A., Dar, G., & Pandith, A. H. (2019). Removal of heavy metal ions from aqueous system by ion-exchange and biosorption methods. *Environmental Chemistry Letters, 17*, 729-754.

Benalia, A., Derbal, K., Baatache, O., Lehchili, C., Khalfaoui, A., & Pizzi, A. (2024). Removal of dyes from water using aluminum-based water treatment sludge as a low-cost coagulant: use of response surface methodology. *Water, 16*(10), 1400.

Boudjemaa, A., Nongwe, I., Mutuma, B., Matsoso, B., Bachari, K., & Coville, N. (2021). TiO2@ hollow carbon spheres: A photocatalyst for hydrogen generation under visible irradiation. *Journal of Photochemistry and Photobiology A: Chemistry, 417*, 113355.

Boudjemaa, A., Rebahi, A., Terfassa, B., Chebout, R., Mokrani, T., Bachari, K., & Coville, N. J. (2015). Fe2O3/carbon spheres for efficient photo-catalytic hydrogen production from water and under visible light irradiation. *Solar Energy Materials and Solar Cells, 140*, 405-411.

Bukhari, S. N. U. S., Shah, A. A., Liu, W., Channa, I. A., Chandio, A. D., Chandio, I. A., & Ibupoto, Z. H. (2024). Activated carbon based TiO2 nanocomposites (TiO2@ AC) used simultaneous adsorption and photocatalytic oxidation for the efficient removal of Rhodamine-B (Rh–B). *Ceramics International, 50*(21), 41285-41298.

Chen, D., Cheng, Y., Zhou, N., Chen, P., Wang, Y., Li, K., . . . Zhang, R. (2020). Photocatalytic degradation of organic pollutants using TiO2-based photocatalysts: A review. *Journal of Cleaner Production, 268*, 121725.

Chen, J., Wang, M., Hu, J., Han, J., Yu, H., & Guo, R. (2022). TiO2 nanosheet/NiO nanorod/poly (dopamine) ternary hybrids towards efficient visible light photocatalysis. *Colloids and Surfaces A: Physicochemical and Engineering Aspects, 637*, 128197.

Cheng, J., Zhan, C., Wu, J., Cui, Z., Si, J., Wang, Q., . . . Turng, L.-S. (2020). Highly efficient removal of methylene blue dye from an aqueous solution using cellulose acetate nanofibrous membranes modified by polydopamine. *Acs Omega, 5*(10), 5389-5400.

Dehno Khalaji, A. (2022). Spherical α Fe2O3 nanoparticles: synthesis and characterization and its photocatalytic degradation of methyl orange and methylene blue. *Physical Chemistry Research, 10*(4), 473-483.

Devi, S., Kumar, S., Kumar, R., Kumar, V., Kumar, A., Singh, O., & Kumar, P. (2025). Efficient α–Fe2O3@ NiO nanocomposites as a photocatalyst for the treatment of hazardous Rose Bengal dye. *Physica B: Condensed Matter, 696*, 416649.

Din, M. I., Khalid, R., Najeeb, J., & Hussain, Z. (2021). Fundamentals and photocatalysis of methylene blue dye using various nanocatalytic assemblies-a critical review. *Journal of Cleaner Production, 298*, 126567.

Ebrahimzadeh, M. A., Mortazavi-Derazkola, S., & Zazouli, M. A. (2020). Eco-friendly green synthesis of novel magnetic Fe3O4/SiO2/ZnO-Pr6O11 nanocomposites for photocatalytic degradation of organic pollutant. *Journal of Rare Earths, 38*(1), 13-20.

Ermanda, Y., Lubis, S., & Ramli, M. (2021). *Preparation and characterization of activated carbon/hematite composite as efficient photocatalyst for naphthol blue black dye degradation.* Paper presented at the AIP Conference Proceedings.

Faheem, M., Iqbal, T., Afsheen, S., Basit, A., Munir, R. M., Khan, M. I., . . . Rizvi, H. I. (2024). A maghemite (γ-Fe2O3) incorporated activated carbon photocatalytic nanocomposite fabricated via Co-precipitation utilized against degradation of methyl orange. *Optical Materials, 157*, 116131.

Farhan, A., Zulfiqar, M., Samiah, Rashid, E. U., Nawaz, S., Iqbal, H. M., . . . Zdarta, J. (2023). Removal of toxic metals from water by nanocomposites through advanced remediation processes and photocatalytic oxidation. *Current Pollution Reports, 9*(3), 338-358.

Fatima, R., Rodríguez-Ortiz, G., Waseem, M., Mahmood, F., Khan, M. A., Bilal, A. S. S., . . . Batool, T. L. (2025). ZnO/α-Fe2O3 nanocomposites as efficient photocatalysts for sustainable hydrogen generation. *Next Materials, 6*, 100486.

Figueroa Campos, G. A., Perez, J. P. H., Block, I., Sagu, S. T., Saravia Celis, P., Taubert, A., & Rawel, H. M. (2021). Preparation of activated carbons from spent coffee grounds and coffee parchment and assessment of their adsorbent efficiency. *Processes, 9*(8), 1396.

Fobiri, G. K. (2022). Synthetic dye application in textiles: A review on the efficacies and toxicities involved. *Text. Leather Rev, 5*, 180-198.

Gebreegziabher, H. G., Yicheneku, Y. B., & Weldegebrieal, G. K. (2024). Synthesis of NiO Nanoparticles using Chemical Precipitation Method for the Photocatalytic Degradation of Methylene Blue Dye.

Goudjil, M. B., Dali, H., Zighmi, S., Mahcene, Z., & Bencheikh, S. E. (2024). Photocatalytic degradation of methylene blue dye with biosynthesized Hematite α-Fe2O3 nanoparticles under UV-Irradiation. *Desalination and Water Treatment, 317*, 100079.

Han, W., Shou, J., Zhu, S., Tu, X., Chen, Y., Sun, C., . . . Zheng, H. (2024). Efficient electron transport between NiO/Fe2O3 by loading amorphous carbon improves photocatalytic degradation property. *Journal of Environmental Chemical Engineering, 12*(1), 111667.

Hanif, M. A., Lee, I., Akter, J., Islam, M. A., Zahid, A. A., Sapkota, K. P., & Hahn, J. R. (2019). Enhanced photocatalytic and antibacterial performance of ZnO nanoparticles prepared by an efficient thermolysis method. *Catalysts, 9*(7), 608.

Hitam, C., & Jalil, A. (2020). A review on exploration of Fe2O3 photocatalyst towards degradation of dyes and organic contaminants. *Journal of environmental management, 258*, 110050.

Hitkari, G., Sandhya, S., Gajanan, P., Shrivash, M., & Deepak, K. (2018). Synthesis of chromium doped cobalt oxide (Cr: Co3O4) nanoparticles by co-precipitation method and enhanced photocatalytic properties in the visible region. *J. Mater. Sci. Eng, 7*(419), 2169-2222.

Holzwarth, U., & Gibson, N. (2011). The Scherrer equation versus the'Debye-Scherrer equation'. *Nature nanotechnology, 6*(9), 534-534.

Hong, J., Bao, J., & Liu, Y. (2025). Removal of Methylene Blue from Simulated Wastewater Based upon Hydrothermal Carbon Activated by Phosphoric Acid. *Water, 17*(5), 733.

Huang, L. Y., Zhang, R. X., Sun, X. J., & Cheng, X. N. (2014). Synthesis and characterization of g-C3N4/α-Fe2O3 composites with enhanced photocatalytic activity. *Key Engineering Materials, 575*, 225-228.

Huang, W., Zhang, D., & Wang, M. (2023). A Review: Research Progress on Photoelectric Catalytic Water Splitting of α-Fe2O3. *Current Nanoscience, 19*(6), 758-769.

Islam, S. U., Latief, U., Ahmad, I., Khan, Z., Ali, J., & Khan, M. S. (2022). Novel NiO/ZnO/Fe2O3 white light-emitting phosphor: facile synthesis, color-tunable photoluminescence and robust photocatalytic activity. *Journal of Materials Science: Materials in Electronics, 33*(29), 23137-23152.

Ismail, A. A., Ali, A. M., Harraz, F. A., Faisal, M., Shoukry, H., & Al-Salami, A. (2019). A facile synthesis of a-Fe2O3/carbon nanotubes and their photocatalytic and electrochemical sensing performances. *International Journal of Electrochemical Science, 14*(1), 15-32.

Iwanow, M., Gärtner, T., Sieber, V., & König, B. (2020). Activated carbon as catalyst support: precursors, preparation, modification and characterization. *Beilstein Journal of Organic Chemistry, 16*(1), 1188-1202.

Kadirova, Z. C., Katsumata, K.-i., Isobe, T., Matsushita, N., Nakajima, A., & Okada, K. (2014). Adsorption and photodegradation of methylene blue with Fe2O3-activated carbons under UV illumination in oxalate solution. *Journal of Environmental Chemical Engineering, 2*(4), 2026-2036.

Keerthana, S., Yuvakkumar, R., Ravi, G., Kumar, P., Elshikh, M. S., Alkhamis, H. H., . . . Velauthapillai, D. (2021). A strategy to enhance the photocatalytic efficiency of α-Fe2O3. *Chemosphere, 270*, 129498.

Khalaf, A., Abu-Dalo, D., & AlShamaileh, E. (2024). Synthesis, Characterization, and Application of Fe2O3 Nanophotocatalyst for the Treatment of Various Pollutants in Aqueous Phase: A Systematic Review. *The Scientific World Journal, 2024*(1), 8644322.

Khan, I., Saeed, K., Zekker, I., Zhang, B., Hendi, A. H., Ahmad, A., . . . Shah, L. A. (2022). Review on methylene blue: Its properties, uses, toxicity and photodegradation. *Water, 14*(2), 242.

Khan, S., Ajmal, Z., Mahmood, S., & ul Haq, M. (2023). Synthesis of mesoporous composites based on α-Fe 2 O 3/NiO nanowires for the photocatalytic degradation of rhodamine B dye. *New Journal of Chemistry, 47*(21), 10333-10346.

Koe, W. S., Lee, J. W., Chong, W. C., Pang, Y. L., & Sim, L. C. (2020). An overview of photocatalytic degradation: photocatalysts, mechanisms, and development of photocatalytic membrane. *Environmental Science and Pollution Research, 27*(3), 2522-2565.

Kumar, Y., Kumar, R., Raizada, P., Khan, A. A. P., Singh, A., Van Le, Q., . . . Singh, P. (2022). Current status of hematite (α-Fe2O3) based Z-scheme photocatalytic systems for environmental and energy applications. *Journal of Environmental Chemical Engineering, 10*(3), 107427.

Li, Y., Zhu, C., Lu, T., Guo, Z., Zhang, D., Ma, J., & Zhu, S. (2013). Simple fabrication of a Fe2O3/carbon composite for use in a high-performance lithium ion battery. *Carbon, 52*, 565-573.

Liu, L., Cui, Z., Feng, B., Sui, M., Huang, H., & Wu, Z. (2024). Synthesis of Fe2O3/TiO2 Photocatalytic Composites for Methylene Blue Degradation as a Novel Strategy for High-Value Utilisation of Iron Scales. *Materials, 17*(18), 4546.

Lopes, J. L., Martins, M. J., Nogueira, H. I., Estrada, A. C., & Trindade, T. (2021). Carbon-based heterogeneous photocatalysts for water cleaning technologies: a review. *Environmental Chemistry Letters, 19*(1), 643-668.

Low, J., Yu, J., Jaroniec, M., Wageh, S., & Al-Ghamdi, A. A. (2017). Heterojunction photocatalysts. *Advanced materials, 29*(20), 1601694.

Lubis, S., Ramli, M., & Ermanda, Y. (2020). *Hydrothermal Synthesis of Activated Carbon/α-Fe2O3 Nanocomposite and Its Application for Removing Tartrazine Dye.* Paper presented at the IOP Conference Series: Materials Science and Engineering.

Mishra, M., & Chun, D.-M. (2015). α-Fe2O3 as a photocatalytic material: A review. *Applied Catalysis A: General, 498*, 126-141.

Moniz, S. J., Shevlin, S. A., An, X., Guo, Z. X., & Tang, J. (2014). Fe2O3–TiO2 nanocomposites for enhanced charge separation and photocatalytic activity. *Chemistry–A European Journal, 20*(47), 15571-15579.

Moorthy, A. K., Rathi, B. G., Shukla, S. P., Kumar, K., & Bharti, V. S. (2021). Acute toxicity of textile dye Methylene blue on growth and metabolism of selected freshwater microalgae. *Environmental Toxicology and Pharmacology, 82*, 103552.

Mou, J., Ren, Y., Wang, J., Wang, C., Zou, Y., Lou, K., . . . Zhang, D. (2022). Nickel oxide nanoparticle synthesis and photocatalytic applications: evolution from conventional methods to novel microfluidic approaches. *Microfluidics and Nanofluidics, 26*(4), 25.

Mummoorthi, G., Shajahan, S., Abu Haija, M., Mahalingam, U., & Rajendran, R. (2022). Synthesis and characterization of ternary α-Fe2O3/NiO/rGO composite for high-performance supercapacitors. *Acs Omega, 7*(31), 27390-27399.

Nassoko, D., Li, Y.-F., Wang, H., Li, J.-L., Li, Y.-Z., & Yu, Y. (2012). Nitrogen-doped TiO2 nanoparticles by using EDTA as nitrogen source and soft template: Simple preparation, mesoporous structure, and photocatalytic activity under visible light. *Journal of Alloys and Compounds, 540*, 228-235.

Nouren, S., Bibi, I., Kausar, A., Sultan, M., Bhatti, H. N., Safa, Y., . . . Iqbal, M. (2024). Green synthesis of CuO nanoparticles using Jasmin sambac extract: Conditions optimization and photocatalytic degradation of Methylene Blue dye. *Journal of King Saud University-Science, 36*(3), 103089.

Nuengmatcha, P., Porrawatkul, P., Chanthai, S., Sricharoen, P., & Limchoowong, N. (2019). Enhanced photocatalytic degradation of methylene blue using Fe2O3/graphene/CuO nanocomposites under visible light. *Journal of Environmental Chemical Engineering, 7*(6), 103438.

Oladoye, P. O., Ajiboye, T. O., Omotola, E. O., & Oyewola, O. J. (2022). Methylene blue dye: Toxicity and potential elimination technology from wastewater. *Results in Engineering, 16*, 100678.

Omanović-Mikličanin, E., Badnjević, A., Kazlagić, A., & Hajlovac, M. (2020). Nanocomposites: a brief review. *Health and Technology, 10*(1), 51-59.

Pagalan Jr, E., Sebron, M., Gomez, S., Salva, S. J., Ampusta, R., Macarayo, A. J., . . . Arazo, R. (2020). Activated carbon from spent coffee grounds as an adsorbent for treatment of water contaminated by aniline yellow dye. *Industrial Crops and Products, 145*, 111953.

Patwa, R., Rohilla, S., & Rani, U. (2024). Characterization of structural and spectroscopic properties of ZnO/Fe_2O_3 nanocomposites. *Ceramics International*, *50*(22), 47268-47277.

Rani, B., Nayak, A. K., & Sahu, N. K. (2022). Fundamentals principle of photocatalysis. In *Nanostructured Materials for Visible Light Photocatalysis* (pp. 1-22): Elsevier.

Ranjithkumar, V., Sangeetha, S., & Vairam, S. (2014). Synthesis of magnetic activated carbon/α-Fe2O3 nanocomposite and its application in the removal of acid yellow 17 dye from water. *Journal of Hazardous Materials*, *273*, 127-135.

Ruhul, A., Kalam, M., Masjuki, H., Fattah, I. R., Reham, S., & Rashed, M. (2015). State of the art of biodiesel production processes: a review of the heterogeneous catalyst. *RSC Advances, 5*(122), 101023-101044.

Sajid, M. M., Ishaq, A. R., Alomayri, T., Zhai, H., & Khan, S. B. (2025). Nanomaterials for Wastewater Treatment. In *Sustainable Use of Wastewater in Agriculture* (pp. 51-67): Apple Academic Press.

Santoshi, T. S., Bharadwaj, S., Varma, M. C., Dhand, V., & Choudary, G. (2024). Structural and magnetic properties of α-Fe2O3 with lithium ferrite prepared using co-precipitation method and annealed at different temperatures. *Chemical Physics Impact*, *9*, 100717.

Shah, R. K. (2023). Efficient photocatalytic degradation of methyl orange dye using facilely synthesized α-Fe2O3 nanoparticles. *Arabian Journal of Chemistry*, *16*(2), 104444.

Shakoor, S., & Nasar, A. (2017). Adsorptive treatment of hazardous methylene blue dye from artificially contaminated water using cucumis sativus peel waste as a low-cost adsorbent. *Groundwater for Sustainable Development*, *5*, 152-159.

Sridharan, S., Perumalsamy, S. V., Kulandaivel, J., Nammalwar, G., Parangusan, H., & Ponnamma, D. (2024). α-Fe2O3/ZnO nanocomposite as an efficient photocatalyst for wastewater treatment and flexible electronic device applications. *Ionics, 30*(2), 1137-1150.

Suresh, R., Gnanasekaran, L., Rajendran, S., Soto-Moscoso, M., Chen, W.-H., Show, P. L., & Khoo, K. S. (2023). Application of nanocomposites in integrated photocatalytic techniques for water pollution remediation. *Environmental Technology & Innovation, 31*, 103149.

Tahir, B., Tahir, M., Alraeesi, A., & Kumar, N. (2024). Photocatalytic Carbon Dioxide Reduction with Water to CO and CH4 over Bio-sludge Modified TiO2 Composite. *Chemical Engineering Transactions, 113*, 193-198.

Tahir, M., Alesayi, M. T., & Al Zahmi, S. (2023). Fabricating Carbon Fibers (CFs)/TiO2 Composite for Photocatalytic Green Hydrogen Production. *Chemical Engineering Transactions, 106*, 679-684.

Taufiq, A., Arista, D., Rachmawati, A., Ramadhani, N., Saputro, R. E., Sunaryono, & Hidayat, N. (2020). *Facile synthesis of α-Fe2O3/TiO2 multiphase nanohybrid particles from local iron sand as antifungal agent.* Paper presented at the AIP Conference Proceedings.

Usman, M., Sarfraz, A., Shafaat, S., Hussain, N., Khan, A. M., Hussain, Z., . . . Shaikh, A. J. (2024). A multiparametric study for size and stability of hybrid Fe2O3-NiO nanoparticles and their statistical transformation. *Particulate Science and Technology*, 1-20.

Valášková, M., Tokarský, J., Pavlovský, J., Prostějovský, T., & Kočí, K. (2019). α-Fe2O3 nanoparticles/vermiculite clay material: structural, optical and photocatalytic properties. *Materials, 12*(11), 1880.

Xie, J., Zhou, Z., Lian, Y., Hao, Y., Li, P., & Wei, Y. (2015). Synthesis of α-Fe2O3/ZnO composites for photocatalytic degradation of pentachlorophenol under UV–vis light irradiation. *Ceramics International, 41*(2), 2622-2625.

Yang, H. (2021). A short review on heterojunction photocatalysts: Carrier transfer behavior and photocatalytic mechanisms. *Materials Research Bulletin, 142*, 111406.

Yang, X., & Wang, D. (2018). Photocatalysis: from fundamental principles to materials and applications. *ACS Applied Energy Materials, 1*(12), 6657-6693.

Yao, C., Wang, Z., Xu, Z., Jiang, B., Yang, Y., & Wang, S. (2023). 2D/2D α-Fe2O3/single-layer MXene Schottky photocatalysis-PMS activation bidirectionally enhanced coupling system for environmental remediation. *Journal of Alloys and Compounds, 941*, 168920.

Yao, L., Leng, Z., Lan, J., Chen, R., & Jiang, J. (2022). Environmental and economic assessment of collective recycling waste plastic and reclaimed asphalt pavement into pavement construction: A case study in Hong Kong. *Journal of Cleaner Production, 336*, 130405.

Yu, L., Wang, Q., Zhang, Z., He, J., Guo, L., Dong, K., & Zhang, Y. (2017). One pot synthesize α-Fe2O3/graphene composites and their photocatalytic properties. *Journal of nanoscience and nanotechnology*, *17*(2), 1350-1355.

Zarei, S., Hasheminiasari, M., Masoudpanah, S., & Javadpour, J. (2022). Photocatalytic properties of ZnO/SnO2 nanocomposite films: role of morphology. *Journal of Materials Research and Technology*, *17*, 2305-2312.

Zhang, J., Dai, M., Zhang, S., Dai, M., Zhang, P., Wang, S., & He, Z. (2022). Recent progress on carbon-nanotube-based materials for photocatalytic applications: a review. *Solar RRL*, *6*(9), 2200243.

Zou, W., Gao, B., Ok, Y. S., & Dong, L. (2019). Integrated adsorption and photocatalytic degradation of volatile organic compounds (VOCs) using carbon-based nanocomposites: A critical review. *Chemosphere*, *218*, 845-859.

Research Fund Acknowledgement

This research is funded by Adama Science and Technology University under the grant number ASTU/SM-R/1156/25, Adama, Ethiopia